Available online at www.sciencedirect.com

SciVerse ScienceDirect

Advances in Space Research 51 (2013) 2093–2111

ADVANCES IN SPACE RESEARCH (a COSPAR publication)

www.elsevier.com/locate/asr

# Optimal guidance based on receding horizon control for low-thrust transfer to libration point orbits

Haijun Peng [a,*], Qiang Gao [a], Zhigang Wu [b], Wanxie Zhong [a]

[a] State Key Laboratory of Structural Analysis for Industrial Equipment, Department of Engineering Mechanics, Dalian University of Technology, Dalian 116024, China

[b] State Key Laboratory of Structural Analysis for Industrial Equipment, School of Aeronautics and Astronautics, Dalian University of Technology, Dalian 116024, China

Received 5 October 2012; received in revised form 7 January 2013; accepted 9 January 2013
Available online 30 January 2013

**Abstract**

This paper addresses the design and computation of a guidance law for a transfer mission from an orbit near the Earth to a halo orbit around the libration point $L_2$ in the Sun–Earth system. The guidance law, which is designed based on receding horizon control and compensates for launch velocity errors that are introduced by inaccuracies of the launch vehicle, is solved using the generating function method. During the design of the closed-loop guidance law, the entire transfer mission, which is considered a nonlinear optimal control problem, is evaluated to obtain a nominal reference trajectory. Using the launch velocity errors and the uncertainty of the model, a spacecraft controlled by the proposed guidance law tracks the reference trajectory. Furthermore, the original Riccati differential equation in the receding horizon control algorithm is replaced by an equivalent convenient form of the Riccati differential equation that is based on the generating function. The high-efficiency solution of the equivalent equation avoids the online direct integration of the original Riccati differential equation, which significantly increases the computational efficiency for the receding horizon control problem. Numerical simulations using a nonlinear bicircular four-body model demonstrate the capabilities of the proposed receding horizon guidance law for the transfer mission. In addition, the generating function method improves the computational efficiency by at least one order of magnitude over the backward sweep method in solving the receding horizon control problem.


*Keywords:* Guidance law; Halo orbit transfer; Bicircular four-body problem; Receding horizon control; Generating function

## 1. Introduction

The exploration of the libration points in space has been accompanied by a rich and growing literature on the design, modeling, and control of a variety of orbits (Gómez et al., 2003; Farquhar et al., 2004; Wang et al., 2007). The halo orbit, which is a special three-dimensional periodic libration point orbit, is useful for performing experiments and observations about the solar and space structure and providing continuous communications between the Earth and the far side of the Moon (Farquhar, 1970a,b; Breakwell et al., 1974; Farquhar et al., 1980; Howell and Pernicka, 1993; Romagnoli and Circi, 2010; Zanzottera et al., 2012). Several space missions have involved libration points, including ISEE-3, Wind, SOHO, ACE and Genesis (Xu and Xu, 2008). The scientific goals of these missions were to examine the structure of the solar wind near the Earth and the shock wave that forms the interface between the solar wind and the Earth's magnetosphere, to monitor the solar wind and associated phenomena near the libration point, and to study the energetic particles from the solar wind, the interplanetary medium, and other sources (Farquhar, 1970a,b; Breakwell et al., 1974; Howell and Pernicka, 1993; Romagnoli and Circi, 2010; Zanzottera et al., 2012). Therefore, the problem of transferring a spacecraft from the Earth to libration point orbits, especially

* Corresponding author. Tel./fax: +86 411 84706574.
*E-mail addresses:* hjpeng@dlut.edu.cn (H. Peng), qgao@dlut.edu.cn (Q. Gao), wuzhg@dlut.edu.cn (Z. Wu), zwoffice@dlut.edu.cn (W. Zhong).

0273-1177/$36.00 © 2013 COSPAR. Published by Elsevier Ltd. All rights reserved.
http://dx.doi.org/10.1016/j.asr.2013.01.013

halo orbits, is an important problem in the field of exploration of the libration point space environment.

Because of the fundamental advantages of the space environment in libration orbits, transfers to these libration point orbits have been widely studied (Gómez et al., 2005; Tantardini et al., 2010). Most of the previous studies on transfer missions have focused on dynamical system models and the type of thrust needed for the transfer. The circular restricted three-body problem (CRTBP) model is the dynamical model that is most commonly used as a foundation for designing transfer orbits (Gómez et al., 2005; Tantardini et al., 2010; Li and Zheng, 2010; Serban et al., 2002). Conley (1968) studied transit, non-transit and asymptotic orbits around the Lagrange point based on the CRTBP model. The effects of the Sun in the Earth–Moon system are ignored, and the effects of the Moon in the Sun–Earth system are also ignored. Hiday-Johnston and Howell (1994) formulated a strategy to design optimal time-fixed impulsive transfers between three-dimensional libration-point orbits based on the elliptic restricted three-body model. The four-body dynamic model was developed to consider the effects of the Sun or the Moon in the design of transfer orbits (Salmani and Büskens, 2011; Cabette and Prado, 2008; Assadian and Pourtakdoust, 2010). The Earth–Moon–Sun–Satellite system is used to study the transit trajectory properties in restricted three- and four-body problems (Circi, 2012).

This paper uses the so-called bicircular four-body model, which places the Sun and Earth in circular orbits about their barycenter and places the Moon in a circular orbit about the barycenter of the entire system (the four-body dynamical model was developed by Salmani and Büskens, 2011). The advantage of this model is that it is more realistic than both the CRTBP of the Sun–Earth system and the CRTBP of the Earth–Moon system. The main disadvantage of this model is that it destroys the periodic solutions that exist in the CRTBP model (Salmani and Büskens, 2011). In addition, the bicircular model is time-periodic with two natural frequencies, and the periodic orbits are replaced by quasi-periodic orbits. In this paper, the halo orbit around the libration point $L_2$ in the Sun–Earth system is considered the objective orbit, so the CRTBP model is considered to generate the periodic halo orbit to overcome the lack of periodic solutions described above.

The choice of a dynamical model is dependent on the requirements of the research mission. A more complex N-body numerical solution and real JPL ephemeris data have higher accuracies than the CRTBP model and the bicircular four-body model for orbit design. Because the purpose of this paper is to design and compute an online guidance law for a transfer mission, the more complex dynamical model requires additional online computational time. In addition, solar pressure, initial velocity errors and the inaccuracies of the thrusts will greatly influence the dynamical model. Therefore, the appropriate accuracy of the dynamical model is used in this paper, and the influences of the modeling uncertainty will be repressed by the online guidance law and not by the more complex dynamical model.

Another important problem is the type of thrust that is used for the transfer to the libration point orbit. Indeed, the dynamical systems approach (Mingotti et al., 2012, 2007; Kechichian, 2001) has been employed as a low-energy transfer method to transfer a spacecraft to a halo orbit with its stable manifold. The Genesis trajectory was the first mission to be fully designed using dynamical system theory (Serban et al., 2002; Howell et al., 1997). However, only the stable manifold associated with the large halo orbit is connected with the parking orbit near the Earth. Furthermore, a trajectory correction maneuver should be implemented during the long-duration transfer to halo orbit. The two most important approaches for trajectory correction are the impulsive maneuver (Li and Zheng, 2010; Rausch, 2005) and low-thrust propulsion (Ozimek and Howell, 2010; Dellnitz et al., 2009). In general, the impulsive maneuver uses a parameter optimization problem to design the thrust and direction variables. Low-thrust propulsion for transfer to a halo orbit can be modeled as a continuous optimal control problem and is more difficult than the parameter optimization problem. While high-thrust impulsive systems have not received sufficient attention over the last decade, many studies have addressed low-thrust spacecraft trajectory optimization. This paper models the transfer problem based on the continuous low-thrust as an optimal control problem that is solved using a symplectic approach (Peng et al., 2011).

In practice, planning the optimal transfer trajectory is not sufficient to implement a transfer mission. Deviations from the required thrust are introduced by inaccuracies in the engine and must be corrected by subsequent maneuvers. In addition, the transfer mission to the libration point orbit is extremely sensitive to launch errors. Therefore, the guidance strategy should compensate for all of the disturbances that cause instabilities in the spacecraft's trajectory. Guidance methods such as predictor–corrector guidance and reference trajectory guidance can be used to correct deviations from the reference nominal trajectory (Tian and Zong, 2011; Arrieta-Camacho and Biegler, 2005). The predictor–corrector guidance method can handle large dispersions and accommodate severe off-nominal conditions. However, for highly constrained guidance scenarios, the computational requirements and convergence guarantees are the most difficult problems (Tian and Zong, 2011). The reference trajectory guidance method is used to track a reference trajectory and is implemented with an online closed-loop guidance law. Receding horizon control has been used as a reference trajectory guidance method for precision entry guidance missions (Lu, 2000, 1999). When using receding horizon control, the optimal control problem is solved over a shorter moving horizon, and the Riccati differential equation needs to be integrated backward over this finite horizon for every time point (Kwon and Pearson, 1977). However, the online computational burden associated with solving the Riccati differen-

tial equation is an impediment for practical applications of the method (Lu, 2000). Nonetheless, the methods described above are important and serve as the foundation for the development of practical and feasible control methods.

Because of the issues described above, a highly efficient numerical algorithm to reduce the online integration burden of the Riccati differential equation has become a key problem for the real-time implementation of receding horizon control. A typical method that is based on the approximate state and control at discrete time points (Lu, 2000) avoids the online integration of the Riccati differential equation. However, the numerical accuracy of the receding horizon control problem is dependent on the approximate state and control variables. Because there are no approximations for the state and control variables, the advantage of the online integration of the Riccati differential equation is its high accuracy. Therefore, this paper first avoids the direct integration of the original Riccati differential equation and then provides an equivalent equation that is expressed by the generating function (Wu and Zhong, 2009; Wu and Mesbahi, 2012). A highly efficient numerical method is proposed for solving the equivalent equation. Not only can the numerical accuracy for receding horizon control be guaranteed, but the online computational efficiency can also be greatly increased. The underlying reason is that in the detailed implementation of the proposed numerical algorithm, the solution to the equivalent equation can be obtained by the combination and separation of formulas of the generating function. This numerical algorithm avoids the online direct integration of the original Riccati differential equation. Meanwhile, the proposed numerical algorithm can ensure the closed-loop stability of the receding horizon control method.

This paper is organized as follows. After a brief introduction to the bicircular four-body problem of the Sun–Earth system, the objective periodic halo orbit is computed using the differential correction algorithm in Section 2. In Section 3, the optimal control problem of the low-thrust transfer mission to the halo orbit is established and solved using a symplectic algorithm. In Section 4, closed-loop guidance based on the receding horizon control method is proposed to correct the trajectory using the linearization equation for the optimal reference trajectory and is solved using the generating function method. In Section 5, numerical simulations are performed with the nonlinear bicircular four-body model. The effects of the initial errors, modeling uncertainty and the guidance law parameters are discussed. The numerical results demonstrate the validity and applicability of the method. Finally, the conclusions are given in Section 6.

## 2. Dynamical model

The main problem addressed in this paper is the design of optimal guidance laws to transfer a spacecraft from an orbit near the Earth to a periodic halo orbit around the libration point $L_2$ in the Sun–Earth system. To increase the precision of the reference transfer trajectories, the bicircular four-body model is used to generate the optimal low-thrust transfer trajectories using the optimal control method. Because the target orbit is a libration point orbit, such as a periodic halo orbit, a brief explanation of the halo orbit is given in this section.

### 2.1. Bicircular four-body model

The bicircular four-body model is more realistic than both the Sun–Earth/Moon and the Earth–Moon three-body models (Salmani and Büskens, 2011). It describes the dynamics observed in systems such as the environment near the Earth and the Moon and describes the motion of a spacecraft of negligible mass under the gravitational force of the Sun, Earth and Moon. The Sun and Earth revolve in circular orbits around their center of mass (barycenter), and the Moon moves in a circular orbit around the center of the Earth (Gómez et al., 2003). Based on the assumptions of the bicircular four-body model, a rotating reference frame $(o,x,y,z)$ is defined with its origin at the $L_2$ point of the Sun–Earth system such that the $x$ unit vector is directed from the Sun towards the Earth, the $y$ unit vector is defined as being normal to the $x$ vector in the plane of the primary orbit and along the prograde rotation direction and the $z$ unit vector completes the right-handed frame and is thus normal to the plane of the primaries' orbits. The motion equations in the bicircular four-body model can be written in dimensionless form as follows (Gómez et al., 2003):

$$\ddot{x} = 2\dot{y} + x - (1-\mu)\frac{(x+\mu)}{r_{PS}^3} - \mu\frac{(x-1+\mu)}{r_{PE}^3} - m_M\frac{(x-x_M)}{r_{PM}^3} \tag{1}$$

$$\ddot{y} = -2\dot{x} + y - (1-\mu)\frac{y}{r_{PS}^3} - \mu\frac{y}{r_{PE}^3} - m_M\frac{(y-y_M)}{r_{PM}^3} \tag{2}$$

$$\ddot{z} = -(1-\mu)\frac{z}{r_{PS}^3} - \mu\frac{z}{r_{PE}^3} - m_M\frac{z}{r_{PM}^3} \tag{3}$$

where

$$r_{PS}^2 = (x+\mu)^2 + y^2 + z^2 \tag{4}$$

$$r_{PE}^2 = (x-1+\mu)^2 + y^2 + z^2 \tag{5}$$

$$r_{PM}^2 = (x-x_M)^2 + (y-y_M)^2 + z^2 \tag{6}$$

The dot represents the time derivative in the rotating frame, $\mu$ is the ratio of the Earth's mass to the sum of the masses of the Earth and the Sun, $r_{PS}$, $r_{PE}$ and $r_{PM}$ are the distances from the spacecraft to the Sun, the Earth and the Moon, respectively, and $m_M$ is the parameter of the Moon in the same nondimensional mass units.

Furthermore, the influence of the Moon's motion can be expressed by

$$x_M = R_M\cos(\omega_M t + \theta_0) \tag{7}$$

$$y_M = R_M\sin(\omega_M t + \theta_0) \tag{8}$$

where the Sun and the Earth hold and the Moon moves about the barycenter of the Sun–Earth system on a circle with radius $R_M$ in nondimensional distance units (Gómez et al., 2003), $\omega_M$ is the angular velocity of the Moon and $\theta_0$ is the initial phase of the Moon.

### 2.2. Halo orbits

The advantage of the bicircular four-body model is that it gives a better approximation of the environment near the Earth; thus, a transfer trajectory that is based on this model will consume less fuel. However, the main disadvantage of this model is that it destroys the particular and periodic solutions of the CRTBP model (Gómez et al., 2003). Therefore, in this paper the CRTBP model is used to compute the periodic libration orbits, i.e., the target halo orbits. The CRTBP model can be obtained easily from the bicircular four-body model as follows (Schaub and Junkins, 2002)

$$\ddot{x} = 2\dot{y} + x - (1-\mu)\frac{(x+\mu)}{r_{PS}^3} - \mu\frac{(x-1+\mu)}{r_{PE}^3} \tag{9}$$

$$\ddot{y} = -2\dot{x} + y - (1-\mu)\frac{y}{r_{PS}^3} - \mu\frac{y}{r_{PE}^3} \tag{10}$$

$$\ddot{z} = -(1-\mu)\frac{z}{r_{PS}^3} - \mu\frac{z}{r_{PE}^3} \tag{11}$$

Halo orbits are special periodic orbits around collinear libration points (Fig. 1) and can be determined using a differential correction algorithm (Richardson, 1980). The initial conditions of these halo orbits can be given as $\mathbf{x}_0 = [x(0), y(0), z(0), \dot{x}(0), \dot{y}(0), \dot{z}(0)]^{\mathrm{T}}$. Because of the orbit's symmetry with respect to the $(x-z)$ plane, we obtain the initial conditions $y(0) = 0$, $\dot{x}(0) = 0$ and $\dot{z}(0) = 0$. A differential correction algorithm can then be applied to determine the other initial conditions. The detailed implementation of halo orbits can be found in Richardson (1980).

Fig. 1(a) and (b) illustrate families of halo orbits around the libration point $L_2$ in the Sun–Earth system. The amplitudes of the orbits range from $1 \times 10^5$ km to $5 \times 10^5$ km in the $z$ direction. Although the sizes of these halo orbits differ widely, the orbital periods are nearly the same (approximately 180 days). Meanwhile, the relative velocities of the two halo orbits are smaller than in the case of two body dynamics.

## 3. Optimal low-thrust transfer to libration point orbits

In this section, we apply the reference trajectory guidance method to establish the controlled nonlinear transfer formulation and then generate the reference optimal low-thrust transfer trajectory using the nonlinear optimal control method.

### 3.1. Problem formulation

The transfer mission from the near-Earth orbit to the halo orbit is formulated as a nonlinear optimal control problem. The objective of the transfer mission is to minimize the energy consumption for a fixed flight time (Ross, 2006), i.e.,

$$J = \frac{1}{2}\int_{t_0}^{t_f} (u_x^2 + u_y^2 + u_z^2)\mathrm{d}t \tag{12}$$

where $u_x$, $u_y$ and $u_z$ are the control variables (acceleration) in the $x$, $y$ and $z$ directions, respectively, $t_0$ is the initial flight time and $t_f$ is the duration of the flight.

By introducing the new variables $x_1 = x$, $x_2 = y$, $x_3 = z$, $x_4 = \dot{x}$, $x_5 = \dot{y}$ and $x_6 = \dot{z}$, the controlled second-order nonlinear dynamical model can be rewritten in the state space form as follows:

$$\dot{x}_1 = x_4 \tag{13}$$

$$\dot{x}_2 = x_5 \tag{14}$$

$$\dot{x}_3 = x_6 \tag{15}$$

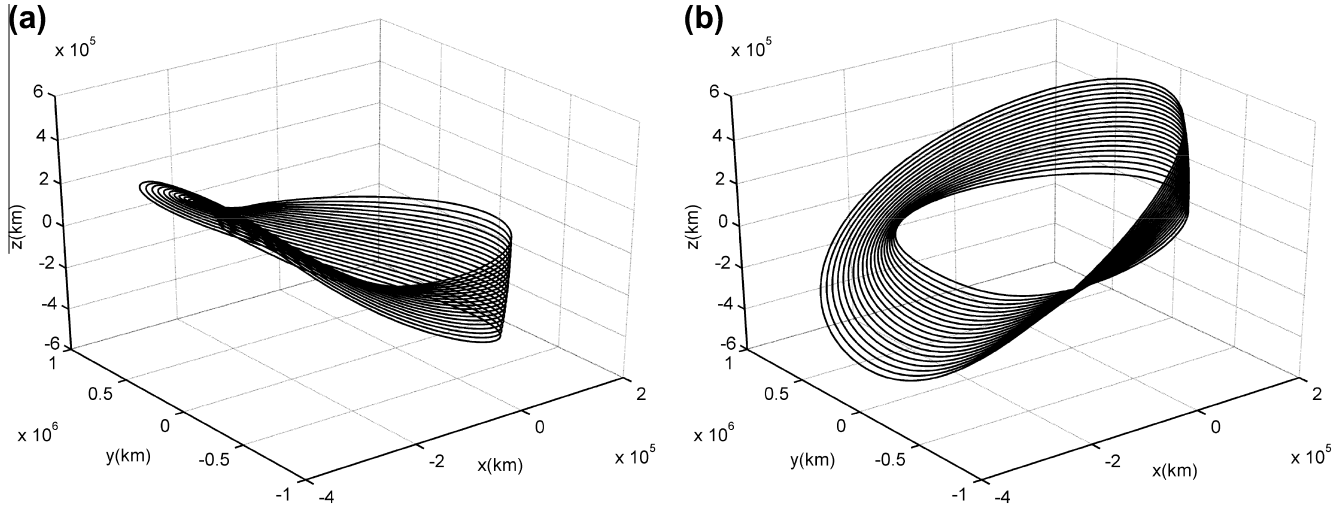


Fig. 1. Families of halo orbits around the libration point $L_2$ in the Sun–Earth system: (a) northern halo orbits and (b) southern halo orbits.

$$\dot{x}_4 = 2x_5 + x_1 - (1-\mu)\frac{(x_1+\mu)}{\bar{r}_{PS}^3} - \mu\frac{(x_1-1+\mu)}{\bar{r}_{PE}^3} - m_M\frac{(x_1-x_M)}{\bar{r}_{PM}^3} + u_x \quad (16)$$

$$\dot{x}_5 = -2x_4 + x_2 - (1-\mu)\frac{x_2}{\bar{r}_{PS}^3} - \mu\frac{x_2}{\bar{r}_{PE}^3} - m_M\frac{(x_2-y_M)}{\bar{r}_{PM}^3} + u_y \quad (17)$$

$$\dot{x}_6 = -(1-\mu)\frac{x_3}{\bar{r}_{PS}^3} - \mu\frac{x_3}{\bar{r}_{PE}^3} - m_M\frac{x_3}{\bar{r}_{PM}^3} + u_z \quad (18)$$

where

$$\bar{r}_{PS}^2 = (x_1+\mu)^2 + x_2^2 + x_3^2 \quad (19)$$

$$\bar{r}_{PE}^2 = (x_1-1+\mu)^2 + x_2^2 + x_3^2 \quad (20)$$

$$\bar{r}_{PM}^2 = (x_1-x_M)^2 + (x_2-y_M)^2 + x_3^2 \quad (21)$$

Meanwhile, the initial and final conditions of the optimal transfer trajectory are given by

$$\mathbf{x}(t_0) = [x_1(t_0), x_2(t_0), x_3(t_0), x_4(t_0), x_5(t_0), x_6(t_0)] \quad (22)$$

$$\mathbf{x}(t_f) = [x_1(t_f), x_2(t_f), x_3(t_f), x_4(t_f), x_5(t_f), x_6(t_f)] \quad (23)$$

The initial position and velocity conditions in Eq. (22) are for the space near the Earth. The final position and velocity conditions in Eq. (23) are for the desired halo orbit around libration point $L_2$ in the Sun–Earth system.

Thus, the optimal control problem for designing the transfer orbit can be summarized as follows. In a given fixed time interval $[t_0, \quad t_f]$, a spacecraft with the dynamical model given by Eqs. (13)–(18) is controlled from the initial conditions Eq. (22) to the final conditions (23) with the minimum energy consumption (12).

### 3.2. Generation of nominal reference trajectory and control

With the nonlinear optimal control model established in the previous section, many numerical methods (Betts, 1998; Conway, 2011; Hull, 1997; Biegler, 2010) can be used to solve the nonlinear optimal control problem and generate the reference trajectories and control histories. These numerical methods are divided into two major classes (Betts, 1998; Conway, 2011): indirect methods and direct methods. The indirect methods transform the optimal control problem into a Hamiltonian boundary value problem (HBVP) by calculus of variations or the maximum principle; the HBVP is then solved using numerical methods, such as the shooting or multiple-shooting methods. The primary advantages of the indirect methods are the high accuracy of the solution and the assurance that the solution satisfies the first-order optimality conditions. However, the indirect methods have several disadvantages, including small radii of convergence, the need to analytically derive the HBVP and the need for an initial guess for the costate. In the direct methods, the optimal control problem is discretized and converted to large-scale parameter optimization problems that can be solved using nonlinear programming methods (Hull, 1997; Biegler, 2010). The direct methods are advantageous to the indirect methods because they have larger radii of convergence and do not require an initial guess for the costate.

The nonlinear optimal control problem has the essential characteristics of a Hamiltonian system. The fundamental property of Hamiltonian systems is that the phase flow is a symplectic transformation. Numerical methods that preserve the symplectic structure are more effective for solving Hamiltonian systems. For example, the symplectic method exhibits excellent energy behavior and accurately reflects the qualitative behavior of the solution. Therefore, we employ a recently developed symplectic numerical method (Peng et al., 2011) to solve the nonlinear optimal control problem in this paper. The nonlinear optimal control problem is transformed to nonlinear algebraic equations by the dual variational principle. The state, control and costate variables can all be obtained from the solutions of nonlinear algebraic equations. The detailed realization can be found in Peng et al. (2011).

We have compared several strategies for the design of transfer trajectories to test the effectiveness of the symplectic numerical method for solving the optimal control problem. We only found detailed information about the design of transfer trajectories to halo orbits around the $L_1$ point for the Sun–Earth three-body system, so we compare the results of our method with the dynamical systems method (Gómez et al., 2005) and the dynamical system method

Table 1
Parameters for generation of nominal reference trajectory and control.

| Parameter | Value | Units |
|---|---|---|
| Mass ratio parameter $\mu$ | 3.034040E−6 | Unitless |
| Mass ratio parameter $m_M$ | 3.694262E−8 | Unitless |
| Orbital parameter $R_M$ | 3.942878E+5 | km |
| Velocity parameter $\omega_M$ | 1.547340E−5 | rad/s |
| Average Sun–Earth distance | 1.4959787E+8 | km |
| Unit time length | 5.0225480E+6 | s |
| Initial position | $[1.4962200992, 0.0001404799, 0.0001228010] \times 10^8$ | km |
| Initial velocity | $[4.4432029400, 2.3224844237, -0.6322604756] \times 10^3$ | m/s |
| Final position | $[1.5058570439, 0, 0.0056593377] \times 10^8$ | km |
| Final velocity | $[0, 4.588948873, 0] \times 10^2$ | m/s |
| Time of fight | 113–123 | day |

Table 2
Performances of the transfer trajectories with different transfer times.

| Transfer time (days) | Velocity increment $\Delta V_{initial}$ (m/s) | Velocity increment $\Delta V_{transfer}$ (m/s) |
|---|---|---|
| 113 | 14.5281 | 133.4435 |
| 115 | 13.5297 | 95.2373 |
| 117 | 12.9250 | 71.6593 |
| 119 | 12.0538 | 73.4220 |
| 121 | 11.5316 | 112.3495 |
| 123 | 10.7767 | 159.3128 |

combined with the optimal control method (Serban et al., 2002). The coordinates of the departure point and the arrival point are taken from Tables 1 and 2 in Gómez et al. (2005), in which the initial condition is not a point of the stable manifold of the halo orbit. Using these parameters, zero initial velocity error and transfer time 173.25 days, the simulation was performed using the Serban et al. (2002), Gómez et al. (2005) and the present method. The transfer trajectory and nominal halo orbit are obtained using the present method and are plotted in Fig. 2. The fuel consumption from Gómez et al. (2005) is 14.1298 m/s, the fuel consumption from Serban et al. (2002) is 13.4831 m/s and the fuel consumption from our method is 16.2790 m/s. The fuel consumption from our method is slightly higher than in the other two methods, which may be a result of the different method used to evaluate fuel consumption. In contrast to the instantaneous velocity changes of the dynamical system method, the control inputs of our method continuously change. Therefore, the evaluation of fuel consumption in our method may have some differences from the other methods. Furthermore, the comparisons of the methods demonstrate the effectiveness of the symplectic numerical method for solving the optimal control problem.

The nominal reference transfer trajectory with the initial conditions given in present Table 1 is also not an orbit of the stable manifold of the halo orbit. Fig. 3 shows the transfer trajectories from the near Earth orbit to the halo orbit around the libration point $L_2$ in the Sun–Earth system obtained using the parameters in Table 1 and zero

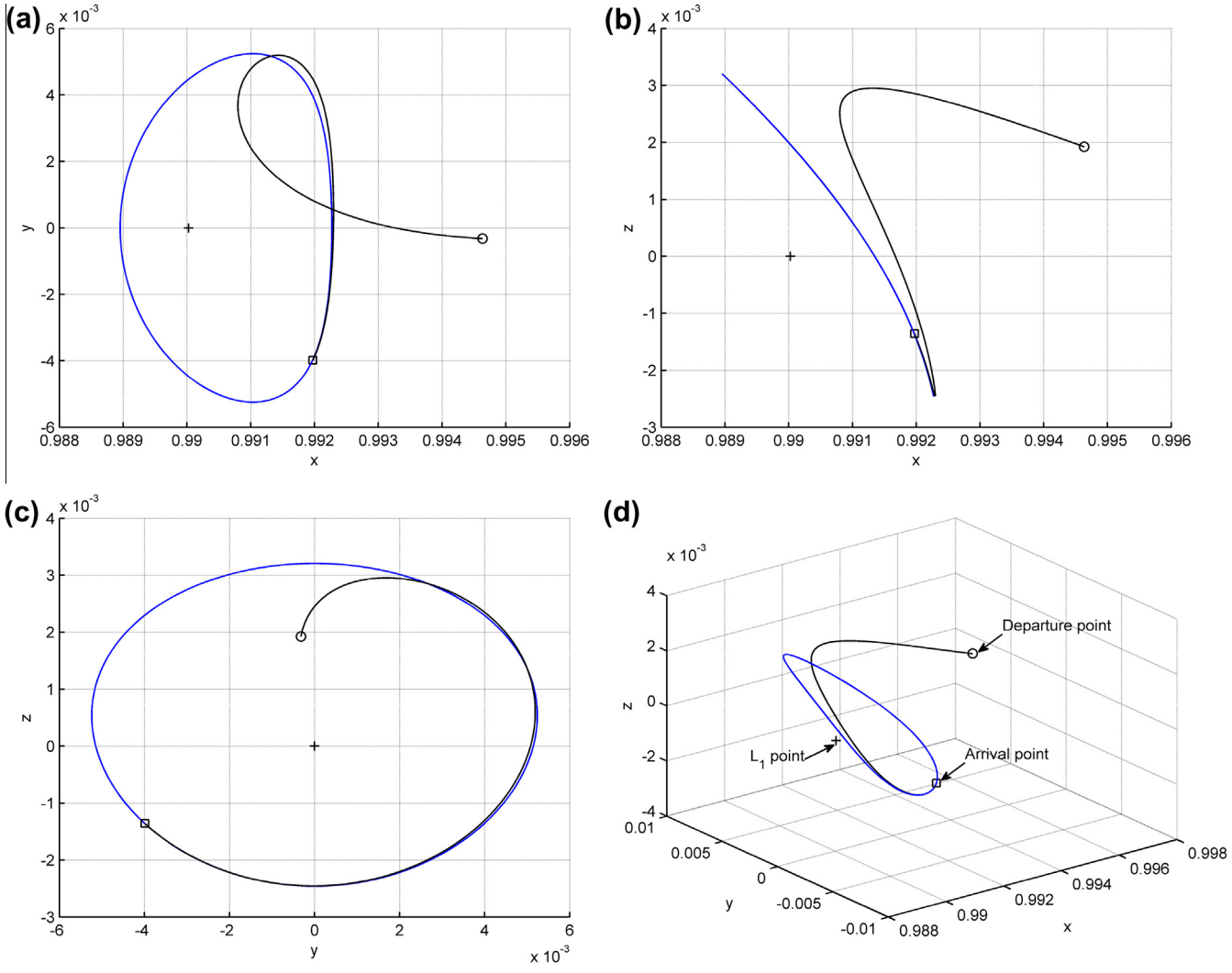


Fig. 2. Transfer trajectories from the low Earth orbit to the halo orbit around the libration point $L_1$ in the Sun–Earth system: (a) $x$–$y$ projection, (b) $x$–$z$ projection, (c) $y$–$z$ projection and (d) 3D space.

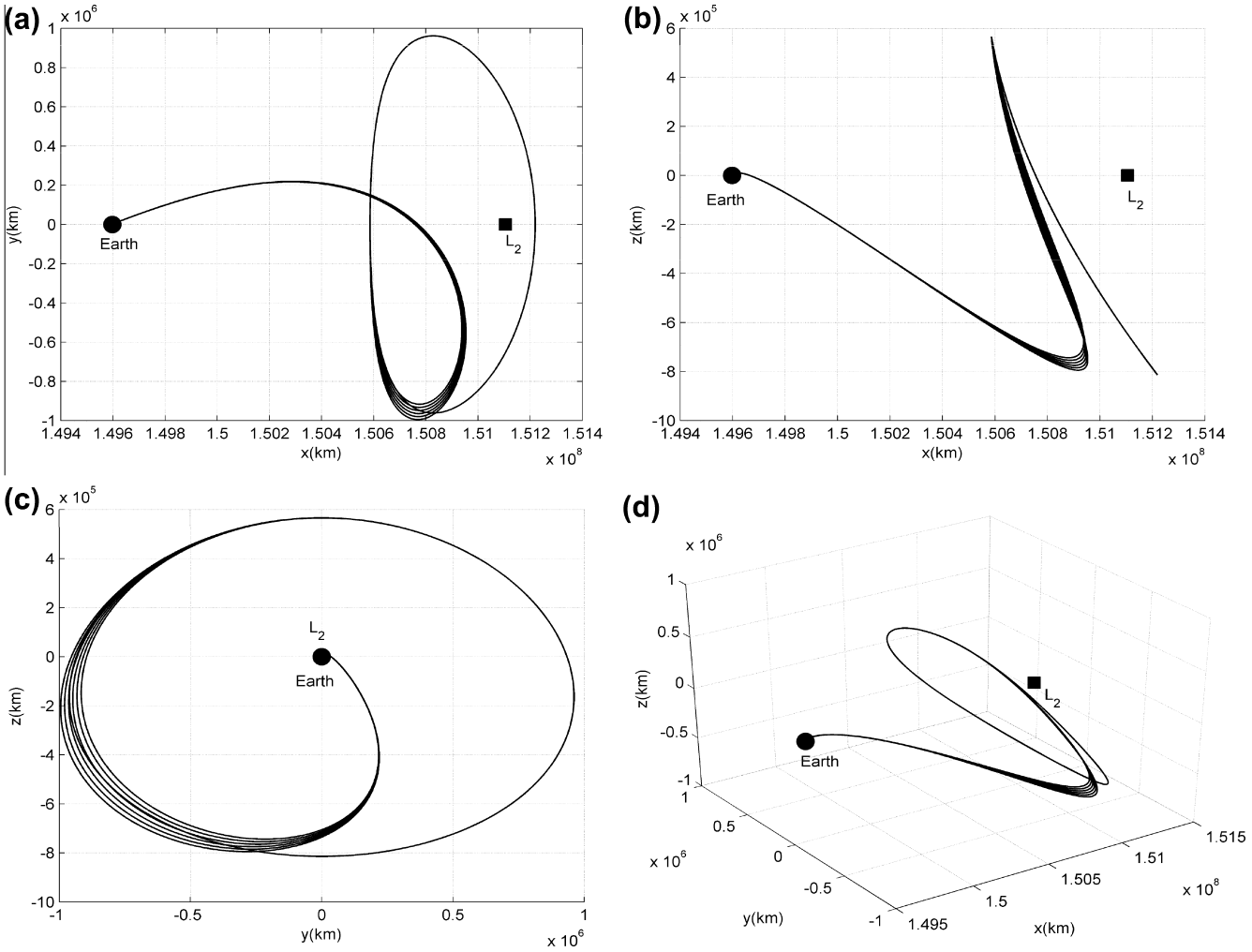


Fig. 3. Transfer trajectories from the low Earth orbit to the halo orbit around the libration point $L_2$ in the Sun–Earth system: (a) $x$–$y$ projection, (b) $x$–$z$ projection, (c) $y$–$z$ projection and (d) 3D space.

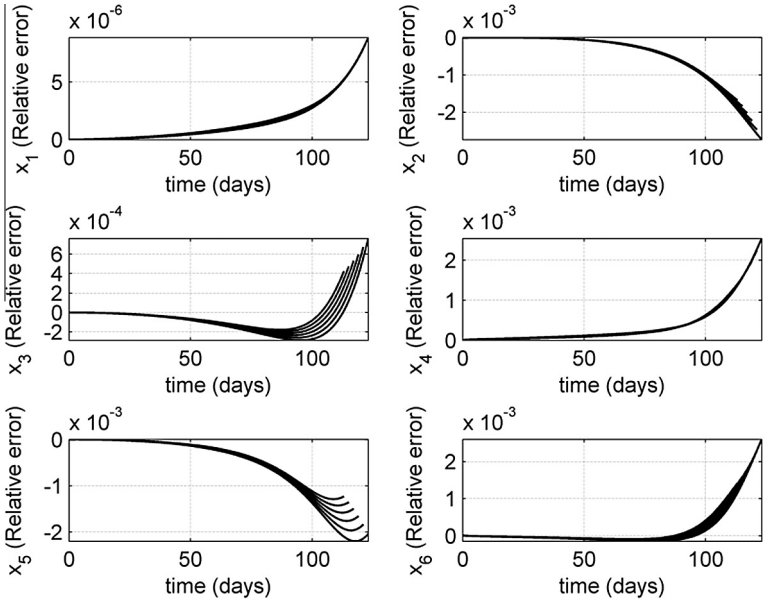


Fig. 4. Relative trajectory deviations compared with the ODE45 results for different flight times.

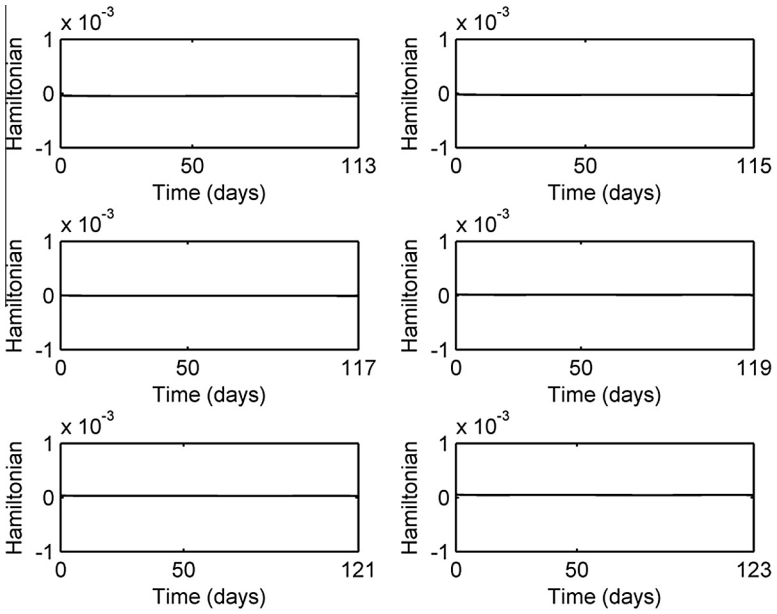


Fig. 5. Hamiltonian function for different flight times.

initial velocity error. The different solid lines plotted in Fig. 3 show the different nominal reference trajectories for different transfer times, i.e. $113, 115, \ldots, 123$ days. To fully describe the performance of the transfer trajectory, the initial velocity increment $\Delta V_{\text{initial}}$ at the beginning of the trajectory (near the Earth) and the velocity increment $\Delta V_{\text{transfer}}$ due to the nominal control during the transfer trajectory should both be given. However, in contrast to the instantaneous velocity changes of the dynamical system method, the control inputs of our method change continuously. In addition, the halo orbit transfer missions must generally correct the launch error within the first 7 days after launch or the velocity change that is required to correct the error will increase beyond the spacecraft's capability (Serban et al., 2002). Therefore, we evaluate the initial velocity change $\Delta V_{\text{initial}}$ within 3 days after launch and the velocity change $\Delta V_{\text{transfer}}$ after 3 days due to the nominal control. The detailed performance of the transfer trajectories with different transfer times are given in Table 2.

Furthermore, the feasibility of the controlled trajectory that was obtained from the symplectic numerical method is independently validated by propagating the states via a separate ordinary differential equation solver (the ODE45 function in Matlab). The relative and absolute errors are both set to $1 \times 10^{-12}$ in the ODE45 function. By interpolating the values of the control variables that are provided by the symplectic numerical method and then integrating the controlled nonlinear differential Eqs. (13)–(18), the relative deviations of the controlled trajectories of the symplectic numerical method are compared with the results of the numerical integration (Fig. 4). The results show that the controlled trajectories obtained using the symplectic numerical method are similar to the trajectories from the numerical integration method and demonstrate that the direct results differ from the integration results by $1 \times 10^{-3}$ to $1 \times 10^{-6}$. To confirm the validity of the symplectic numerical method for solving this type of orbital transfer problem, different Hamiltonian functions for different times of flight are shown in Fig. 5.

## 4. Closed-loop guidance law using the receding horizon control method

The purpose of designing a closed-loop guidance law is to correct deviations from the space mission trajectory that are produced by environmental disturbances and other perturbations. In this section, the closed-loop guidance law is developed based on the receding horizon control method and the known reference trajectory. The original Riccati differential equation in the receding horizon control is then replaced by an equivalent convenient form of the Riccati differential equation that is based on the generating function. Finally, a high-efficiency numerical method based on the generating function is developed to solve the equivalent Riccati differential equation and avoid the online integration of the original Riccati differential equation.

### 4.1. Closed-loop guidance law

The closed-loop guidance law is designed based on the trajectory error with respect to the reference trajectory and the receding horizon control method. Thus, the linearized dynamical model given by Eqs. (13)–(18) with respect to the reference trajectory is derived as

$$\delta\dot{\mathbf{x}}(t) = \mathbf{A}(t)\delta\mathbf{x}(t) + \mathbf{B}\delta\mathbf{u}(t) \tag{24}$$

$$\mathbf{A}(t) = \begin{bmatrix} \mathbf{0}_3 & \mathbf{I}_3 \\ \mathbf{\Pi} & \mathbf{J} \end{bmatrix} \tag{25}$$

$$\mathbf{B}=\begin{bmatrix}0&0&0&1&0&0\\0&0&0&0&1&0\\0&0&0&0&0&1\end{bmatrix}^{\mathrm{T}} \tag{26}$$

where $\mathbf{I}_3$ and $\mathbf{0}_3$ are the three-dimensional identity matrix and three-dimensional zero matrix, respectively. In addition,

$$\mathbf{J}=\begin{bmatrix}0&2&0\\-2&0&0\\0&0&0\end{bmatrix},\quad \mathbf{\Pi}=\begin{bmatrix}\Pi_{11}&\Pi_{12}&\Pi_{13}\\\Pi_{21}&\Pi_{22}&\Pi_{23}\\\Pi_{31}&\Pi_{32}&\Pi_{33}\end{bmatrix}$$

$$\begin{aligned}\Pi_{11}&=1-\frac{1-\mu}{r_{\mathrm{PS}}^3}+\frac{3(1-\mu)(x_1+\mu)^2}{r_{\mathrm{PS}}^5}-\frac{\mu}{r_{\mathrm{PE}}^3}\\&\quad+\frac{3\mu(x_1-1+\mu)^2}{r_{\mathrm{PE}}^5}-\frac{m_M}{r_{\mathrm{PM}}^3}+\frac{3m_M(x_1-x_M)^2}{r_{\mathrm{PM}}^5}\\\Pi_{12}&=\frac{3(1-\mu)(x_1+\mu)x_2}{r_{\mathrm{PS}}^5}+\frac{3\mu(x_1-1+\mu)x_2}{r_{\mathrm{PE}}^5}\\&\quad+\frac{3m_M(x_1-x_M)(x_2-y_M)}{r_{\mathrm{PM}}^5}\\\Pi_{13}&=\frac{3(1-\mu)(x_1+\mu)x_3}{r_{\mathrm{PS}}^5}+\frac{3\mu(x_1-1+\mu)x_3}{r_{\mathrm{PE}}^5}\\&\quad+\frac{3m_M(x_1-x_M)x_3}{r_{\mathrm{PM}}^5}\\\Pi_{21}&=\frac{3(1-\mu)x_2(x_1+\mu)}{r_{\mathrm{PS}}^5}+\frac{3\mu x_2(x_1-1+\mu)}{r_{\mathrm{PE}}^5}\\&\quad+\frac{3m_M(x_2-y_M)(x_1-x_M)}{r_{\mathrm{PM}}^5}\\\Pi_{22}&=1-\frac{1-\mu}{r_{\mathrm{PS}}^3}+\frac{3(1-\mu)x_2^2}{r_{\mathrm{PS}}^5}-\frac{\mu}{r_{\mathrm{PE}}^3}+\frac{3\mu x_2^2}{r_{\mathrm{PE}}^5}-\frac{m_M}{r_{\mathrm{PM}}^3}\\&\quad+\frac{3m_M(x_2-y_M)^2}{r_{\mathrm{PM}}^5}\\\Pi_{23}&=\frac{3(1-\mu)x_2x_3}{r_{\mathrm{PS}}^5}+\frac{3\mu x_2x_3}{r_{\mathrm{PE}}^5}+\frac{3m_M(x_2-y_M)x_3}{r_{\mathrm{PM}}^5}\\\Pi_{31}&=\frac{3(1-\mu)x_3(x_1+\mu)}{r_{\mathrm{PS}}^5}+\frac{3\mu x_3(x_1-1+\mu)}{r_{\mathrm{PE}}^5}\\&\quad+\frac{3m_Mx_3(x_1-x_M)}{r_{\mathrm{PM}}^5}\\\Pi_{32}&=\frac{3(1-\mu)x_2x_3}{r_{\mathrm{PS}}^5}+\frac{3\mu x_2x_3}{r_{\mathrm{PE}}^5}+\frac{3m_Mx_3(x_2-y_M)}{r_{\mathrm{PM}}^5}\\\Pi_{33}&=-\frac{1-\mu}{r_{\mathrm{PS}}^3}+\frac{3(1-\mu)x_3^2}{r_{\mathrm{PS}}^5}-\frac{\mu}{r_{\mathrm{PE}}^3}+\frac{3\mu x_3^2}{r_{\mathrm{PE}}^5}-\frac{m_M}{r_{\mathrm{PM}}^3}+\frac{3m_Mx_3^2}{r_{\mathrm{PM}}^5}\end{aligned}$$

Eq. (24) is a linear time-varying system in which the values of the coefficient matrix $\mathbf{A}(t)$ are determined by the state histories of the reference trajectory. The symbols $\delta\mathbf{x}$ and $\delta\mathbf{u}$ are the deviations from the reference trajectory and control, respectively. Many methods can be used for controlling the linear time-varying system described above; one popular approach is gain scheduling. In this method, controllers are designed at several points in time. The method requires the repetitive solving of algebraic Riccati equations, and the gains are then interpolated over time. The fundamental issue is that closed-loop stability cannot be theoretically guaranteed by such a gain-scheduled controller without additional conditions (Lu, 2000). Because the linear time-varying system is continuously regulated based on the updated information, the receding horizon control approach is more robust. Most importantly, the closed-loop stability has been proved theoretically (Lu, 2000). Therefore, the receding horizon control approach is used to control the linear time-varying system.

The receding horizon control problem at any fixed time $t \geqslant 0$ is defined to be an optimal control problem in which the performance index

$$J=\int_t^{t+T}\left[\delta\mathbf{x}^{\mathrm{T}}(\tau)\mathbf{Q}\delta\mathbf{x}(\tau)+\delta\mathbf{u}^{\mathrm{T}}(\tau)\mathbf{R}\delta\mathbf{u}(\tau)\right]\mathrm{d}\tau \tag{27}$$

is minimized for a chosen time interval $\delta \leqslant T \leqslant \infty$ ($\delta$ is a positive constant) subject to the linear time-varying dynamical system Eq. (24) and the constraint $\mathbf{x}(t+T)=0$. The symbols $\mathbf{Q}\in\mathbb{R}^{n\times n}$ and $\mathbf{R}\in\mathbb{R}^{m\times m}$ are the weighted matrices. The weighted matrix $\mathbf{Q}$ is a non-negative symmetric matrix, and $\mathbf{R}$ is the positive definite symmetric matrix.

The main idea of receding horizon control is to solve the optimal control $\delta\mathbf{u}_{\mathrm{optm}}(t)$ for the problem described above in one time interval $[t, t+T]$ using the current state $\delta\mathbf{x}(t)$ as the initial condition. Only the first data $\delta\mathbf{u}_{\mathrm{optm}}(t)$ is employed as the current control input to the system; the remainder of the control $\delta\mathbf{u}_{\mathrm{optm}}(t)$ is discarded. For the next time $t$, the solution process described above is repeated, and the control input is recomputed (Lu, 2000). A detailed computation of a control input obtained using a similar receding horizon control strategy is given by Lu (2000):

$$\delta\mathbf{u}^*(t)=-\mathbf{R}^{-1}\mathbf{B}^{\mathrm{T}}\mathbf{P}^{-1}(t,t+T)\delta\mathbf{x}(t) \tag{28}$$

where $\mathbf{P}(t, t+T)$ satisfies the matrix Riccati differential Eq. (29) at any time $\tau\in(t,t+T)\triangleq(t,t_T)$ and

$$\begin{aligned}\dot{\mathbf{P}}(\tau,t_T)&=\mathbf{A}(\tau)\mathbf{P}(\tau,t_T)+\mathbf{P}(\tau,t_T)\mathbf{A}^{\mathrm{T}}(\tau)\\&\quad+\mathbf{P}(\tau,t_T)\mathbf{Q}\mathbf{P}(\tau,t_T)-\mathbf{B}\mathbf{R}^{-1}\mathbf{B}^{\mathrm{T}}\end{aligned} \tag{29}$$

with the boundary condition $\mathbf{P}(t_T, t_T)=\mathbf{P}(t+T, t+T)=\mathbf{0}$.

Assuming that the matrix pair $\{\mathbf{A}(t), \mathbf{B}(t)\}$ is uniformly completely controllable, the controlled system under control law (i.e., Eq. (28)) is uniformly asymptotically stable (Lu, 2000), and the Riccati differential equation has a stable solution. From a practical point of view, the online integration of the Riccati differential equation (i.e., Eq. (29)) for every time $t \geqslant 0$ poses a significant online computational burden if the control strategy Eq. (28) is implemented. The key problem of receding horizon control is the efficiency of real-time computation. Therefore, in the following sections, the receding horizon control is devel-

oped in terms of the generating function of the Hamiltonian system, and the online integration of the Riccati differential equation is avoided to increase the efficiency in real-time computation.

### 4.2. Numerical algorithm for solving the receding horizon control problem

Park et al. (2006) stated that one generating function can be defined for the linear Hamiltonian system as follows:

$$\mathcal{F}(\delta\mathbf{x}_0,\delta\boldsymbol{\lambda},t;t_0)=\frac{1}{2}\begin{Bmatrix}\delta\mathbf{x}_0\\ \delta\boldsymbol{\lambda}\end{Bmatrix}^{\mathrm{T}}\begin{bmatrix}\mathbf{F}_{xx}(t;t_0) & \mathbf{F}_{x\lambda}(t;t_0)\\ \mathbf{F}_{\lambda x}(t;t_0) & -\mathbf{F}_{\lambda\lambda}(t;t_0)\end{bmatrix}\begin{Bmatrix}\delta\mathbf{x}_0\\ \delta\boldsymbol{\lambda}\end{Bmatrix} \tag{30}$$

where $\mathbf{F}_{xx}(t;t_0)$, $\mathbf{F}_{x\lambda}(t;t_0)=\mathbf{F}_{\lambda x}^{\mathrm{T}}(t;t_0)$ and $\mathbf{F}_{\lambda\lambda}(t;t_0)$ are coefficient matrices of $\mathcal{F}(\mathbf{x}_0,\boldsymbol{\lambda},t;t_0)$, $\delta\mathbf{x}_0$ is the initial state deviation from the reference trajectory and $\delta\boldsymbol{\lambda}$ is the costate variables deviation. The generating function $\mathcal{F}(\delta\mathbf{x}_0,\delta\boldsymbol{\lambda},t;t_0)$ satisfies the following Hamilton–Jacobi partial differential equation (Park et al., 2006):

$$\frac{\partial\mathcal{F}(\delta\mathbf{x}_0,\delta\boldsymbol{\lambda},t;t_0)}{\partial t}+\mathcal{H}\left(-\frac{\partial\mathcal{F}(\delta\mathbf{x}_0,\delta\boldsymbol{\lambda},t;t_0)}{\partial(\delta\boldsymbol{\lambda})},\delta\boldsymbol{\lambda},t\right)=0 \tag{31}$$

and the initial costate $\delta\boldsymbol{\lambda}$&$_0$ and state variable $\delta\mathbf{x}$can be derived from

$$\delta\mathbf{x}=-\frac{\partial\mathcal{F}(\delta\mathbf{x}_0,\delta\boldsymbol{\lambda},t;t_0)}{\partial(\delta\boldsymbol{\lambda})}=-\mathbf{F}_{\lambda x}(t;t_0)\delta\mathbf{x}_0+\mathbf{F}_{\lambda\lambda}(t;t_0)\delta\boldsymbol{\lambda} \tag{32}$$

$$\boldsymbol{\lambda}_0\frac{\mathcal{F}(\mathbf{x}_0,\boldsymbol{\lambda},t;t_0)}{\delta(\mathbf{x}_0)}\mathbf{F}_{xx}(t;t_0)\mathbf{x}_0\mathbf{F}_x(t;t_0)\delta\boldsymbol{\lambda} \tag{33}$$

where $\mathcal{H}$

where $\mathcal{H}$ is the Hamiltonian function and can be expressed as

$$\mathcal{H}(\delta\mathbf{x},\delta\boldsymbol{\lambda},t)=\frac{1}{2}\begin{Bmatrix}\delta\mathbf{x}(t)\\ \delta\boldsymbol{\lambda}(t)\end{Bmatrix}^{\mathrm{T}}\begin{bmatrix}\mathbf{Q} & \mathbf{A}^{\mathrm{T}}(t)\\ \mathbf{A}(t) & -\mathbf{B}\mathbf{R}^{-1}\mathbf{B}^{\mathrm{T}}\end{bmatrix}\begin{Bmatrix}\delta\mathbf{x}(t)\\ \delta\boldsymbol{\lambda}(t)\end{Bmatrix} \tag{34}$$

According to the Park et al. (2006), the Hamiltonian function (34) can be formulated with the generating function using Eqs. (32) and (33) as follows:

$$\mathcal{H}(\delta\mathbf{x},\delta\boldsymbol{\lambda},t)=\frac{1}{2}\begin{Bmatrix}\delta\mathbf{x}_0\\ \delta\boldsymbol{\lambda}\end{Bmatrix}^{\mathrm{T}}\begin{bmatrix}-\mathbf{F}_{x\lambda}(t;t_0) & \mathbf{0}\\ \mathbf{F}_{\lambda\lambda}(t;t_0) & \mathbf{I}\end{bmatrix}\begin{bmatrix}\mathbf{Q} & \mathbf{A}^{\mathrm{T}}(t)\\ \mathbf{A}(t) & -\mathbf{B}\mathbf{R}^{-1}\mathbf{B}^{\mathrm{T}}\end{bmatrix}\times\begin{bmatrix}-\mathbf{F}_{\lambda x}(t;t_0) & \mathbf{F}_{\lambda\lambda}(t;t_0)\\ \mathbf{0} & \mathbf{I}\end{bmatrix}\begin{Bmatrix}\delta\mathbf{x}_0\\ \delta\boldsymbol{\lambda}\end{Bmatrix} \tag{35}$$

By substituting the generating function (30) and the Hamiltonian function (35) into the Hamilton–Jacobi partial differential Eq. (31) and comparing the same terms of the coefficient matrices, the following ordinal differential equation is obtained:

$$-\dot{\mathbf{F}}_{\lambda\lambda}(t;t_0)+\mathbf{A}(t)\mathbf{F}_{\lambda\lambda}(t;t_0)+\mathbf{F}_{\lambda\lambda}(t;t_0)\mathbf{A}^{\mathrm{T}}(t)+\mathbf{F}_{\lambda\lambda}(t;t_0)\mathbf{Q}\mathbf{F}_{\lambda\lambda}(t;t_0)-\mathbf{B}\mathbf{R}^{-1}\mathbf{B}^{\mathrm{T}}=\mathbf{0} \tag{36}$$

Eqs. (29) and (36) have the same form and are both Riccati differential equations. However, Eq. (36) is derived differently than Eq. (29) and is expressed with the generating function. Therefore, solving Eq. (36) is equivalent to solving Eq. (29). Once the solution of the Riccati differential equation is computed, the feedback control law Eq. (28) of the receding horizon control problem is obtained. The solutions of the Riccati differential equation (i.e., Eq. (36)) are obtained by the combination and separation of the coefficient matrices of the generating function ($\mathcal{F}(\mathbf{x}_0,\boldsymbol{\lambda},t;t_0)$), which replace the online integration process.

In view of Eqs. (32) and (33), the relationship of the state and costate can be expressed in terms of the coefficient matrices of the generating function; i.e., Eqs. (32) and (33) have an equivalent expression:

$$\begin{Bmatrix}\delta\mathbf{x}(t)\\ \delta\boldsymbol{\lambda}(t)\end{Bmatrix}=\begin{bmatrix}-\mathbf{F}_{\lambda x}(t;t_0)-\mathbf{F}_{\lambda\lambda}(t;t_0)\mathbf{F}_{x\lambda}^{-1}(t;t_0)\mathbf{F}_{xx}(t;t_0) & -\mathbf{F}_{\lambda\lambda}(t;t_0)\mathbf{F}_{x\lambda}^{-1}(t;t_0)\\ -\mathbf{F}_{x\lambda}^{-1}(t;t_0)\mathbf{F}_{xx}(t;t_0) & -\mathbf{F}_{x\lambda}^{-1}(t;t_0)\end{bmatrix}\times\begin{Bmatrix}\delta\mathbf{x}(t_0)\\ \delta\boldsymbol{\lambda}(t_0)\end{Bmatrix} \tag{37}$$

In a numerical algorithm, the simulation time domain $[t_0,\quad t_f]$ is divided into $N$ time intervals of equal time step size $\eta$, i.e., $t_0=0, t_1=\eta,\ldots,t_k=k\eta,\ldots,t_f=N\eta$. Hence, the state transfer matrices in the intervals $(t_{k-1};t_k)$, $(t_k;t_{k+1})$ and $(t_{k-1};t_{k+1})$ can be obtained from Eq. (37) as follows:

$$\boldsymbol{\Phi}(t_k;t_{k-1})=\begin{bmatrix}-(\mathbf{F}_{\lambda x}(t_k;t_{k-1})+\mathbf{F}_{\lambda\lambda}(t_k;t_{k-1})\mathbf{F}_{x\lambda}^{-1}(t_k;t_{k-1})\mathbf{F}_{xx}(t_k;t_{k-1})) & -\mathbf{F}_{\lambda\lambda}(t_k;t_{k-1})\mathbf{F}_{x\lambda}^{-1}(t_k;t_{k-1})\\ -\mathbf{F}_{x\lambda}^{-1}(t_k;t_{k-1})\mathbf{F}_{xx}(t_k;t_{k-1}) & -\mathbf{F}_{x\lambda}^{-1}(t_k;t_{k-1})\end{bmatrix} \tag{38}$$

$$\boldsymbol{\Phi}(t_{k+1};t_k)=\begin{bmatrix}-(\mathbf{F}_{\lambda x}(t_{k+1};t_k)+\mathbf{F}_{\lambda\lambda}(t_{k+1};t_k)\mathbf{F}_{x\lambda}^{-1}(t_{k+1};t_k)\mathbf{F}_{xx}(t_{k+1};t_k)) & -\mathbf{F}_{\lambda\lambda}(t_{k+1};t_k)\mathbf{F}_{x\lambda}^{-1}(t_{k+1};t_k)\\ -\mathbf{F}_{x\lambda}^{-1}(t_{k+1};t_k)\mathbf{F}_{xx}(t_{k+1};t_k) & -\mathbf{F}_{x\lambda}^{-1}(t_{k+1};t_k)\end{bmatrix} \tag{39}$$

$$\mathbf{\Phi}(t_{k+1};t_{k-1})=\begin{bmatrix}-(\mathbf{F}_{\lambda x}(t_{k+1};t_{k-1})+\mathbf{F}_{\lambda\lambda}(t_{k+1};t_{k-1})\mathbf{F}_{x\lambda}^{-1}(t_{k+1};t_{k-1})\mathbf{F}_{xx}(t_{k+1};t_{k-1})) & -\mathbf{F}_{\lambda\lambda}(t_{k+1};t_{k-1})\mathbf{F}_{x\lambda}^{-1}(t_{k+1};t_{k-1})\\ -\mathbf{F}_{x\lambda}^{-1}(t_{k+1};t_{k-1})\mathbf{F}_{xx}(t_{k+1};t_{k-1}) & -\mathbf{F}_{x\lambda}^{-1}(t_{k+1};t_{k-1})\end{bmatrix} \tag{40}$$

According to the properties of the state transfer matrices,

$$\mathbf{\Phi}(t_{k+1},t_{k-1})=\mathbf{\Phi}(t_{k+1},t_k)\mathbf{\Phi}(t_k,t_{k-1}) \tag{41}$$

Eqs. (38)–(40) are substituted into Eq. (41), and the combination of the interval coefficient matrices of the generating function are formulated as

$$\mathbf{F}_{xx}(t_{k+1};t_{k-1})=\mathbf{F}_{xx}(t_k;t_{k-1})+\mathbf{F}_{x\lambda}(t_k;t_{k-1})\mathbf{\Psi}\mathbf{F}_{xx}(t_{k+1};t_k)\mathbf{F}_{\lambda x}(t_k;t_{k-1}) \tag{42}$$

$$\mathbf{F}_{x\lambda}(t_{k+1};t_{k-1})=-\mathbf{F}_{x\lambda}(t_k;t_{k-1})\mathbf{\Psi}\mathbf{F}_{x\lambda}(t_{k+1};t_k) \tag{43}$$

$$\mathbf{F}_{\lambda\lambda}(t_{k+1};t_{k-1})=\mathbf{F}_{\lambda\lambda}(t_{k+1};t_k)+\mathbf{F}_{\lambda x}(t_{k+1};t_k)\mathbf{F}_{\lambda\lambda}(t_k;t_{k-1})\mathbf{\Psi}\mathbf{F}_{x\lambda}(t_{k+1};t_k) \tag{44}$$

$$\mathbf{\Psi}=(\mathbf{I}+\mathbf{F}_{xx}(t_{k+1};t_k)\mathbf{F}_{\lambda\lambda}(t_k;t_{k-1}))^{-1} \tag{45}$$

The combination formulas (i.e., Eqs. (42)–(44) show that if the coefficient matrices of the generating function are known for time intervals $(t_{k-1};\ t_k)$ and $(t_k;\ t_{k+1})$, then the coefficient matrices of the generating function for a larger time interval $(t_{k-1};\ t_{k+1})$ can be evaluated by the combination formulas.

Similarly, according to the properties of the state transition matrices,

$$\mathbf{\Phi}(t_{k+1},t_k)=\mathbf{\Phi}(t_{k+1},t_{k-1})\mathbf{\Phi}^{-1}(t_k,t_{k-1}) \tag{46}$$

Eqs. (38)–(40) are substituted into Eq. (46), and the separation of the interval coefficient matrices of the generating function are formulated as

$$\mathbf{F}_{x\lambda}(t_{k+1};t_k)=(\mathbf{\Omega}\mathbf{F}_{\lambda\lambda}(t_k;t_{k-1})-\mathbf{F}_{x\lambda}(t_k;t_{k-1}))^{-1}\mathbf{F}_{x\lambda}(t_{k+1};t_{k-1}) \tag{47}$$

$$\mathbf{F}_{xx}(t_{k+1};t_k)=-\mathbf{F}_{x\lambda}(t_{k+1};t_k)\mathbf{F}_{x\lambda}^{-1}(t_{k+1};t_{k-1})\mathbf{\Omega} \tag{48}$$

$$\mathbf{F}_{\lambda\lambda}(t_{k+1};t_k)=\mathbf{F}_{\lambda\lambda}(t_{k+1};t_{k-1})+\mathbf{F}_{\lambda x}(t_{k+1};t_{k-1})\mathbf{F}_{\lambda x}^{-1}(t_k;t_{k-1})\mathbf{F}_{\lambda\lambda}(t_k;t_{k-1})\mathbf{F}_{x\lambda}(t_{k+1};t_k) \tag{49}$$

$$\mathbf{\Omega}=(\mathbf{F}_{xx}(t_{k+1};t_{k-1})-\mathbf{F}_{xx}(t_k;t_{k-1}))\mathbf{F}_{\lambda x}^{-1}(t_k;t_{k-1}) \tag{50}$$

The separation formulas (i.e., Eqs. (47)–(49)) show that if the coefficient matrices of the generating function are known for time intervals $(t_{k-1};\ t_k)$ and $(t_{k-1};\ t_{k+1})$, then the coefficient matrices of the generating function for a smaller time interval $(t_k;\ t_{k+1})$ can be evaluated by the separation formulas.

Based on the discussion presented above, the online integration of the Riccati differential equation is replaced by one combination formula and one separation formula in every time step. The only problem for the solutions of the Riccati differential equation is the unknown coefficient matrices of the generating function. Therefore, the relationship between the generating function and the state transition matrix is derived, and the key point of solving the generating function is converted to the solving of the state transition matrix.

The state transfer matrix of the linear Hamiltonian system (34) can be given by

$$\mathbf{\Phi}(t;t_0)=\begin{bmatrix}\mathbf{\Phi}_{xx}(t;t_0) & \mathbf{\Phi}_{x\lambda}(t;t_0)\\ \mathbf{\Phi}_{\lambda x}(t;t_0) & \mathbf{\Phi}_{\lambda\lambda}(t;t_0)\end{bmatrix} \tag{51}$$

which relates the states and costates at time $t$ with the initial states and costate by

$$\begin{Bmatrix}\delta\mathbf{x}(t)\\ \delta\boldsymbol{\lambda}(t)\end{Bmatrix}=\begin{bmatrix}\mathbf{\Phi}_{xx}(t;t_0) & \mathbf{\Phi}_{x\lambda}(t;t_0)\\ \mathbf{\Phi}_{\lambda x}(t;t_0) & \mathbf{\Phi}_{\lambda\lambda}(t;t_0)\end{bmatrix}\begin{Bmatrix}\delta\mathbf{x}(t_0)\\ \delta\boldsymbol{\lambda}(t_0)\end{Bmatrix} \tag{52}$$

The state transfer matrix of the linear Hamiltonian system is a symplectic matrix, i.e.

$$\mathbf{\Phi}^{\mathrm{T}}(t;t_0)\mathbf{J}\mathbf{\Phi}(t;t_0)=\mathbf{J} \tag{53}$$

where $\mathbf{J}$ is a unitary symplectic matrix.

According to Eq. (37), the state transfer matrix can be expressed in terms of the generating function. Comparing Eq. (37) with Eq. (52) gives

$$\mathbf{F}_{xx}(t;t_0)=\mathbf{\Phi}_{\lambda\lambda}^{-1}(t;t_0)\mathbf{\Phi}_{\lambda x}(t;t_0) \tag{54}$$

$$\mathbf{F}_{x\lambda}(t;t_0)=-\mathbf{\Phi}_{\lambda\lambda}^{-1}(t;t_0) \tag{55}$$

$$\mathbf{F}_{\lambda x}(t;t_0)=-\mathbf{\Phi}_{xx}(t;t_0)+\mathbf{\Phi}_{x\lambda}(t;t_0)\mathbf{\Phi}_{\lambda\lambda}^{-1}(t;t_0)\mathbf{\Phi}_{\lambda x}(t;t_0) \tag{56}$$

$$\mathbf{F}_{\lambda\lambda}(t;t_0)=\mathbf{\Phi}_{x\lambda}(t;t_0)\mathbf{\Phi}_{\lambda\lambda}^{-1}(t;t_0) \tag{57}$$

The inverse of the partitioned matrix $\mathbf{\Phi}_{\lambda\lambda}(t;t_0)$ exists in Eqs. (54)–(57). The length of the two adjacent time points $(t;\ t_0)$ cannot be made arbitrarily large because the columns of $\mathbf{\Phi}_{\lambda\lambda}(t;t_0)$ become more linearly dependent as the interval $(t;\ t_0)$ increases (Davison and Maki, 1973). If the columns of matrix $\mathbf{\Phi}_{\lambda\lambda}(t;t_0)$ are linearly dependent, the inverse of matrix $\mathbf{\Phi}_{\lambda\lambda}(t;t_0)$ does not exist. Consequently, if the length of interval $(t;\ t_0)$ is small, the inverse of matrix $\mathbf{\Phi}_{\lambda\lambda}(t;t_0)$ always exists.

Eqs. (54)–(57) relate the coefficient matrices of the generating functions and the state transfer matrices of the linear Hamiltonian system. Using this relationship and based on the symplecticity of the state transfer matrix, we employ a structure-preserving numerical algorithm (Hairer et al., 2006) to solve the state transfer matrix and then to solve the generating function accurately and efficiently.

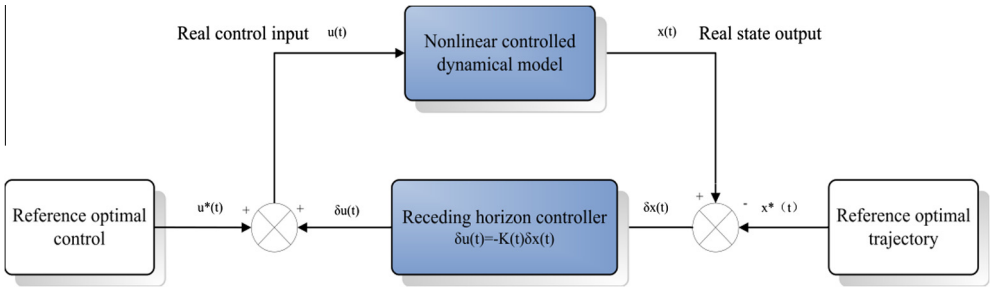


Fig. 6. Simulation process of a spacecraft with a guidance law transferring to a halo orbit.

## 5. Numerical simulations

In this section, numerical simulations are used to validate the effectiveness of the guidance law that is based on receding horizon control. While transferring from the near-Earth orbit to the halo orbit, the spacecraft's deviations are corrected by this guidance law under the assumption of a bicircular four-body model. The detailed simulation process is shown in Fig. 6.

Fig. 6 shows that the optimal reference trajectory $\mathbf{x}^*(t)$ and the reference optimal control $\mathbf{u}^*(t)$ are calculated first. The closed-loop guidance law is then designed based on the receding horizon control and the linearized dynamical model from Eqs. (13)–(18) with respect to the optimal reference trajectory. The real control input is obtained by combining the feedback control variable $\delta\mathbf{u}(t)$ and the reference optimal control variable $\mathbf{u}^*(t)$; i.e., $\mathbf{u}(t) = \mathbf{u}^*(t) + \delta\mathbf{u}(t)$. The real state $\mathbf{x}(t)$ is found by entering the real control input into the nonlinear controlled dynamical model Eqs. (13)–(18). Finally, the deviation $\delta\mathbf{x}(t)$ at the next time point is generated by $\delta\mathbf{x}(t) = \mathbf{x}(t) - \mathbf{x}^*(t)$. This process is repeated until the end of the simulation.

To measure the fuel expenditure for the transfer process, the velocity increment $\Delta V$ is defined as (Kulkarni et al., 2006)

$$\Delta V_x = \int_{t_0}^{t_f} |u_x| \mathrm{d}t, \Delta V_y = \int_{t_0}^{t_f} |u_y| \mathrm{d}t, \Delta V_z = \int_{t_0}^{t_f} |u_z| \mathrm{d}t \quad (58)$$

$$\Delta V = \Delta V_x + \Delta V_y + \Delta V_z \quad (59)$$

where the fuel expenditure $\Delta V$ is in units of meters per second. To measure the final relative position and velocity errors with the closed-loop guidance law, the position error $\Delta e_p$ and the velocity error $\Delta e_v$ are defined as

$$\Delta e_p = \max\left(|x(t_f) - x^*(t_f)|, |y(t_f) - y^*(t_f)|, |z(t_f) - z^*(t_f)|\right) \quad (60)$$

$$\Delta e_v = \max(|\dot{x}(t_f) - \dot{x}^*(t_f)|, |\dot{y}(t_f) - \dot{y}^*(t_f)|, |\dot{z}(t_f) - \dot{z}^*(t_f)|) \quad (61)$$

where $x(t_f)$, $y(t_f)$ and $z(t_f)$ represent the actual final position, while $x^*(t_f)$, $y^*(t_f)$ and $z^*(t_f)$ are the reference final position in the $x$, $y$ and $z$ directions. The final velocity error is defined similarly in Eq. (61). The final relative position error $\Delta e_p$ is in units of kilometers, and the final velocity error is in units of meters per second.

### 5.1. Effect of initial injection error

The initial injection condition is important for the precision and quality of a spacecraft's transfer mission. Two types of injection error, i.e., the deterministic injection error and the stochastic injection error, are used in the numerical simulations.

For the deterministic injection error, the actual departure velocity from the orbit near the Earth has been modified using the following formula (Gómez et al., 2005):

$$\mathbf{v}(0) = \mathbf{v}_0^*\left(1 + \frac{\varepsilon}{\|\mathbf{v}_0^*\|}\right) \quad (62)$$

where $\varepsilon$ is a parameter that varies between 0 m/s and 10 m/s, $\mathbf{v}_0^*$ is the reference initial departure velocity and $\mathbf{v}(0)$ is the actual departure velocity.

The other related parameters in the numerical simulations are chosen as follows. The duration of the flight is 120 days; the receding horizon control parameter is $T = 12$ days; the initial position is given in Table 1. The fuel consumptions, i.e., the velocity changes obtained by the numerical simulations, are given in Table 3. $\Delta V_x$, $\Delta V_y$, $\Delta V_z$ and $\Delta V$ are velocity changes from the nominal trajectory due to the nominal control, and $\Delta\bar{V}_x, \Delta\bar{V}_y, \Delta\bar{V}_z and \Delta\bar{V}$ are the velocity changes due to additional guidance control for the initial velocity errors. Table 3 shows that increases of the parameter $\varepsilon$, i.e., the errors of the initial velocity, increase the fuel expenditures.

The transfer trajectories and the reference optimal transfer trajectories obtained by increasing the initial velocity error to 100 m/s and increasing the receding horizon control parameter to $T = 40$ days are plotted in Fig. 7, and the actual control histories and the reference optimal control histories for these parameters are plotted in Fig. 8, in which the dashed lines are the actual transfer trajectories and control histories with initial velocity error, and the solid lines are the normal reference transfer trajectories and control histories without initial velocity error. The actual trajectories diverged from the reference trajectories in the middle portion of the transfer process. Therefore, the perturbation of the initial velocity condition has a large effect on the transfer process. However, the actual trajectories are very similar to the reference trajectories in the final part of transfer, which indicates that a

Table 3
Velocity increments changing with the different parameter $\varepsilon$.

| Parameter $\varepsilon$ | Velocity increment | | Velocity increment | | Velocity increment | | Velocity increment | |
|---|---|---|---|---|---|---|---|---|
| | $\Delta V_x$ | $\Delta \bar{V}_x$ | $\Delta V_y$ | $\Delta \bar{V}_y$ | $\Delta V_z$ | $\Delta \bar{V}_z$ | $\Delta V$ | $\Delta \bar{V}$ |
| 0 | 62.5871 | 0.6986 | 21.2506 | 0.4031 | 17.9597 | 0.5146 | 101.7974 | 1.6163 |
| 1 | 63.9670 | 0.9475 | 21.9286 | 0.4987 | 18.3234 | 0.2893 | 104.2190 | 1.7354 |
| 2 | 65.3464 | 2.1813 | 22.6089 | 1.0470 | 18.9107 | 1.1133 | 106.8659 | 4.3416 |
| 3 | 66.7253 | 3.6935 | 23.2907 | 1.7409 | 19.5212 | 1.7257 | 109.5372 | 7.1602 |
| 4 | 68.1038 | 5.2061 | 23.9738 | 2.4359 | 20.1321 | 2.3416 | 112.2097 | 9.9836 |
| 5 | 69.4818 | 6.7185 | 24.6580 | 3.1310 | 20.7432 | 2.9587 | 114.8830 | 12.8082 |
| 6 | 70.8593 | 8.2307 | 25.3429 | 3.8259 | 21.3547 | 3.5764 | 117.5569 | 15.6330 |
| 7 | 72.2364 | 9.7426 | 26.0284 | 4.5208 | 21.9664 | 4.1944 | 120.2312 | 18.4578 |
| 8 | 73.6130 | 11.2541 | 26.7146 | 5.2154 | 22.5783 | 4.8125 | 122.9059 | 21.2821 |
| 9 | 74.9892 | 12.7652 | 27.4011 | 5.9099 | 23.1905 | 5.4307 | 125.5807 | 24.1058 |
| 10 | 76.3648 | 14.2758 | 28.0878 | 6.6041 | 23.8028 | 6.0489 | 128.2554 | 26.9288 |

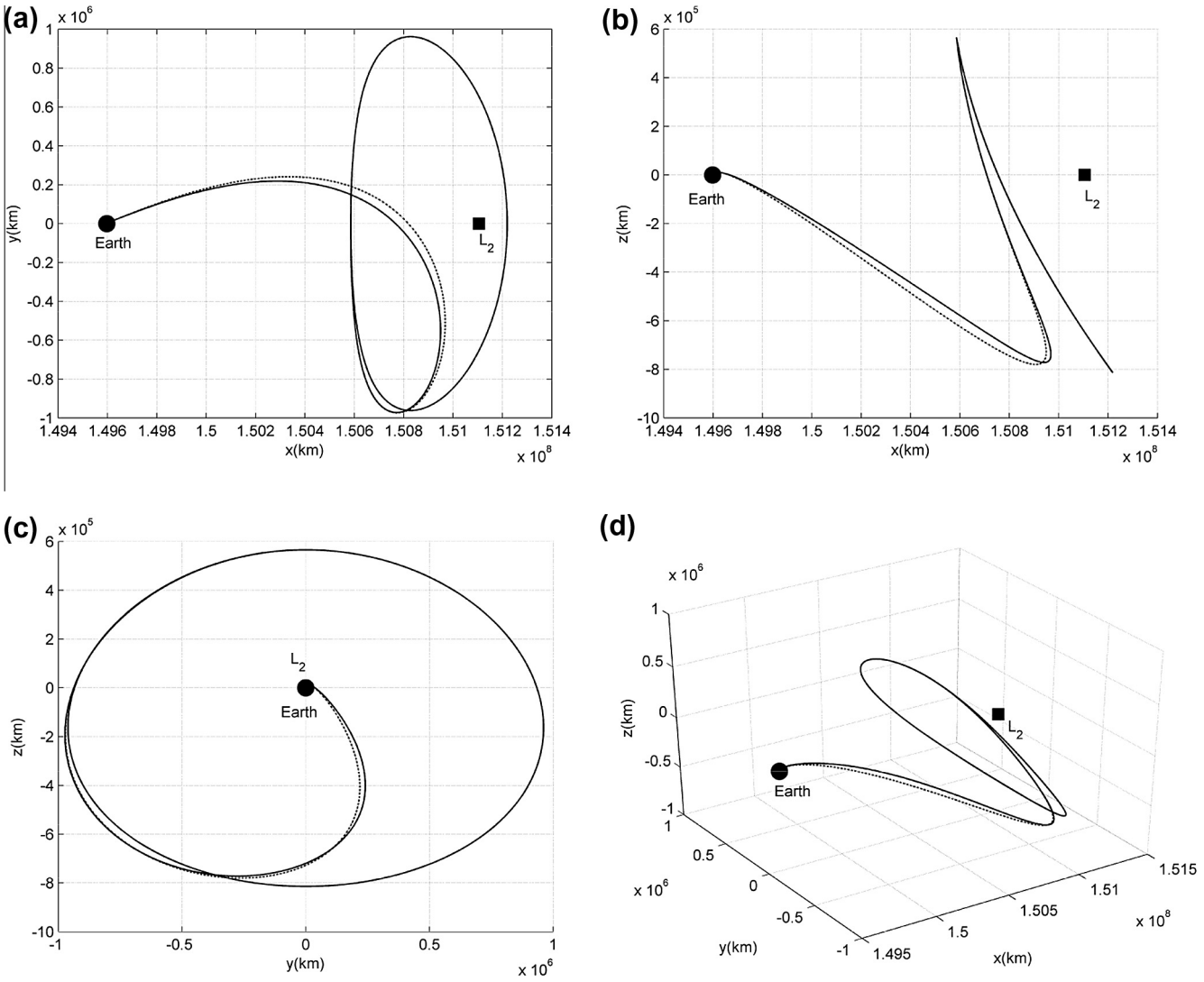


Fig. 7. Actual transfer trajectory (dashed line) and reference optimal transfer trajectory (solid line): (a) $x$–$y$ projection, (b) $x$–$z$ projection, (c) $y$–$z$ projection and (d) 3D space.

spacecraft that uses the proposed guidance law can track the desired reference trajectories even in the presence of the initial errors.

The wide range of uncertainties in the initial condition was also considered. Numerical simulations were performed to verify the performance of the proposed guidance law using the Monte Carlo method with stochastic injec-

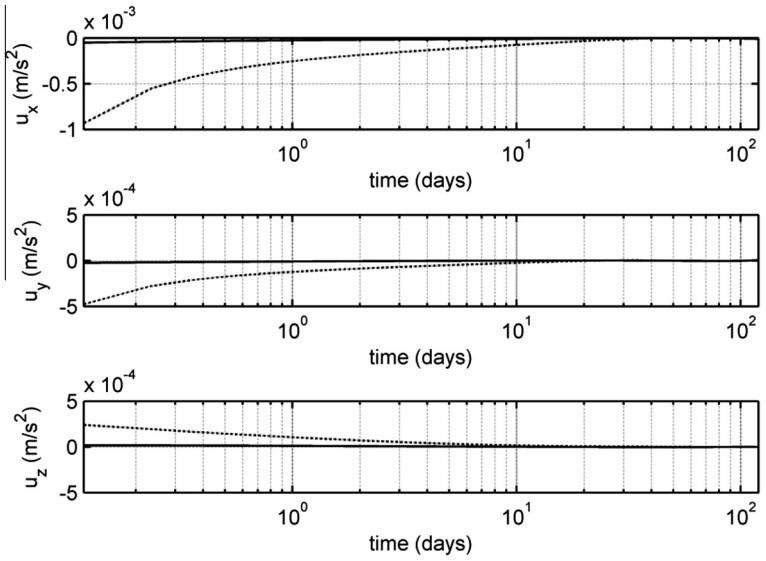


Fig. 8. Actual control histories (dashed line) and reference optimal control histories (solid line).

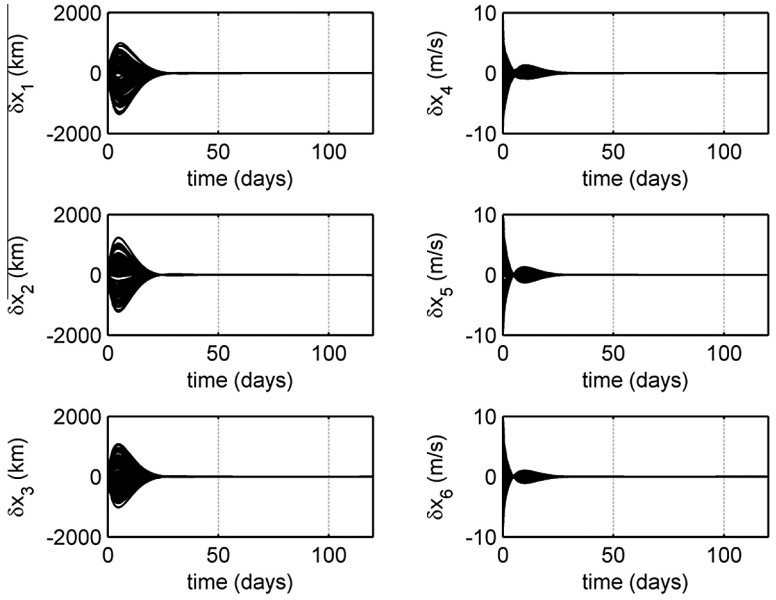


Fig. 9. Errors from the optimal reference trajectory based on stochastic velocity errors.

tion errors between $-10$ m/s and 10 m/s. One hundred simulations are shown in Fig. 9. All of the deviations caused by the stochastic injection errors rapidly converged to zero. Therefore, the guidance law proposed in this paper based on the receding horizon control method is robust and effective.

### 5.2. Effect of modeling uncertainty

In the previous section, the present guidance law was shown to be robust with respect to initial injection errors. In addition, the modeling uncertainty, which includes factors such as solar pressure and other ephemeris dynamics, will influence the orbit transfer mission. Because the present guidance law is designed based on a linear time-varying model that is linearized to the bicircular four-body model, the complex ephemeris dynamics model will generate small errors in the linear time-varying model. To validate the robustness of the present guidance law with such uncertainty, small perturbations from the reference values are added to the time-varying system matrix $\mathbf{A}(t)$ in Eq. (24).

The flight time in the numerical simulations is 120 days, the receding horizon control parameter is $T = 12$ days and the initial velocity errors are all 10 m/s (i.e., 10 m/s is added to the initial velocities $\dot{x}(0), \dot{y}(0)$ and $\dot{z}(0)$). The velocity changes and the final position (velocity) errors with the modeling uncertainties of $\pm 5\%$–$\pm 20\%$ obtained from the numerical simulations are given in Table 4. Figs. 10 and 11 show the position and velocity errors from the optimal reference trajectory with a $\pm 20\%$ model uncertainty, and

Table 4
The effect of model uncertainty for velocity increment and final position/velocity errors.

| Model uncertainty $\Delta\mathbf{A}$ | Velocity increment $\Delta V$ (m/s) | Final position error $\Delta e_p$ (km) | Final velocity error $\Delta e_v$ (m/s) |
|---|---|---|---|
| 0 | 120.8811 | 4.7228 | 0.0025 |
| +5% | 116.8203 | 3.5198 | 0.0020 |
| −5% | 125.0188 | 4.9349 | 0.0026 |
| +10% | 112.8646 | 5.8267 | 0.0035 |
| −10% | 129.1957 | 4.5905 | 0.0025 |
| +15% | 109.1778 | 3.1324 | 0.0016 |
| −15% | 133.3755 | 4.7528 | 0.0025 |
| +20% | 110.1330 | 5.0265 | 0.0027 |
| −20% | 137.5282 | 4.6498 | 0.0025 |

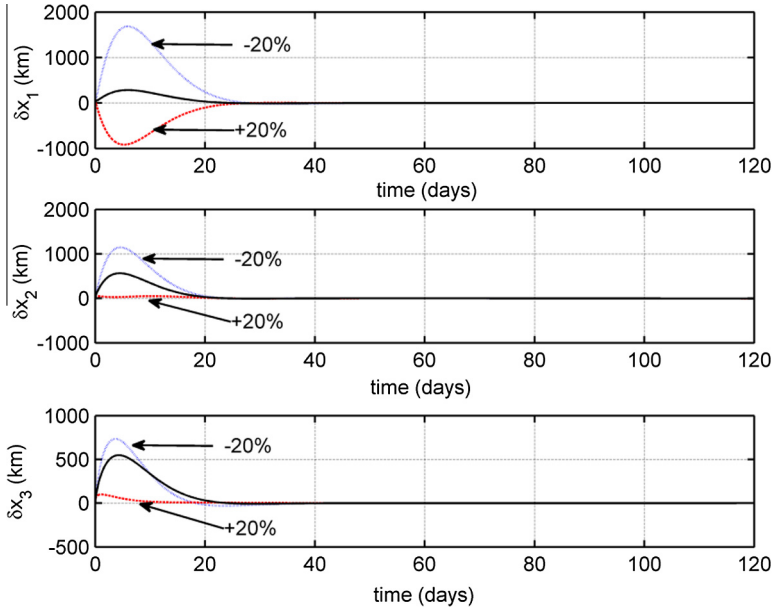


Fig. 10. Position errors from the optimal reference trajectory with model uncertainty.

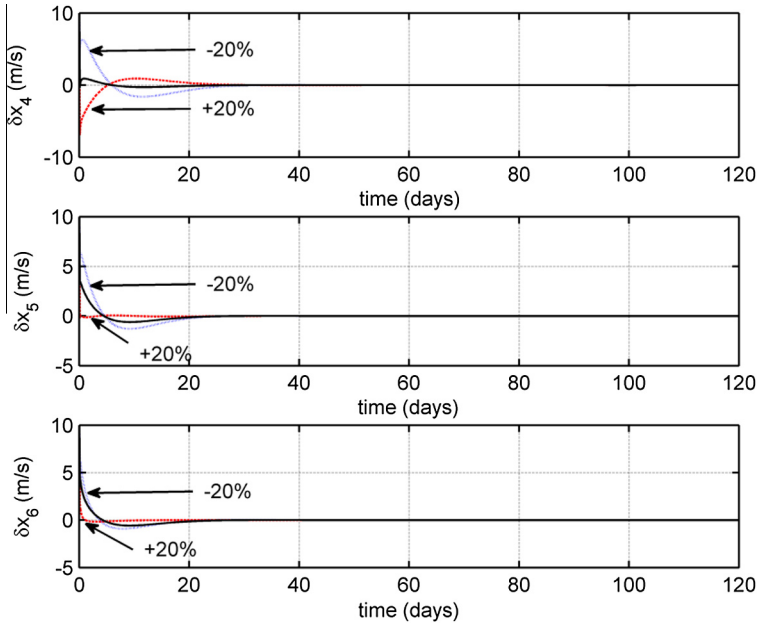


Fig. 11. Velocity errors from the optimal reference trajectory with model uncertainty.

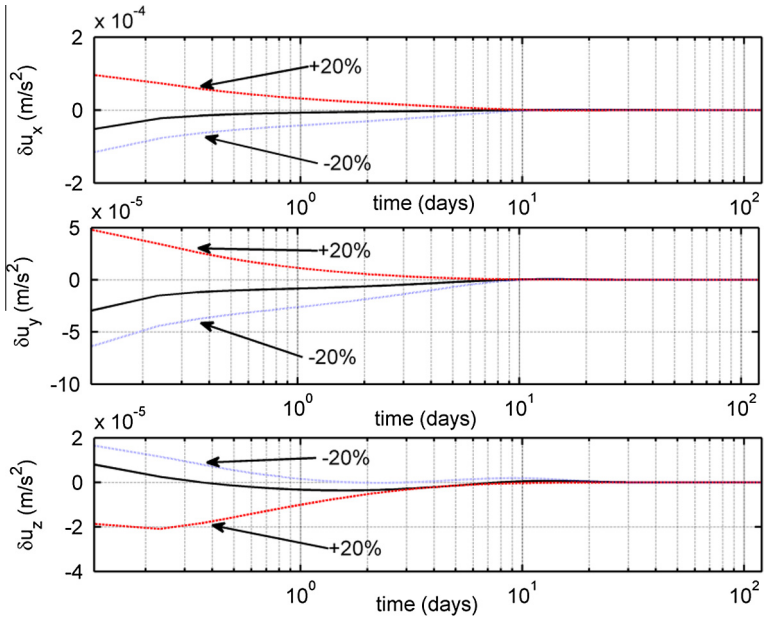


Fig. 12. Control errors from the optimal reference control with model uncertainty.

Table 5
The comparisons between the proposed method and the backward sweep method.

| Parameter $T$ (day) | CPU time $T_{cpu}$ (s) | | Velocity increment $\Delta V$ (m/s) | | Final position error $\Delta e_p$ (km) | | Final velocity error $\Delta e_v$ (m/s) | |
|---|---|---|---|---|---|---|---|---|
| | GF | BS | GF | BS | GF | BS | GF | BS |
| 1 | 3.71 | 41.47 | 147.2161 | 135.5798 | 0.0328 | 0.0291 | 5.4475e−5 | 5.0922e−5 |
| 2 | 3.67 | 41.65 | 132.7274 | 135.2843 | 0.1203 | 0.1385 | 1.1010e−4 | 1.1673e−4 |
| 3 | 3.69 | 41.85 | 123.1537 | 142.7726 | 0.2127 | 0.3038 | 1.8595e−4 | 2.1881e−4 |
| 4 | 3.71 | 41.65 | 116.0734 | 127.8883 | 0.4590 | 0.5649 | 3.3765e−4 | 3.7627e−4 |
| 5 | 3.72 | 45.31 | 112.8173 | 145.4822 | 0.5847 | 0.8615 | 4.4841e−4 | 5.5053e−4 |
| 10 | 3.67 | 46.20 | 118.7869 | 207.0493 | 3.8201 | 3.3551 | 0.0021 | 0.0019 |
| 20 | 3.78 | 47.92 | 126.8184 | 162.7748 | 12.3315 | 11.1271 | 0.0071 | 0.0053 |
| 30 | 3.73 | 53.73 | 131.9519 | 179.8914 | 19.5670 | 11.2277 | 0.0175 | 0.0212 |
| 60 | 3.74 | 62.40 | 140.6725 | 197.0870 | 298.1657 | 713.5882 | 0.1317 | 0.4081 |
| 120 | 3.78 | 99.98 | 144.2283 | 208.1440 | 2018.40 | 5705.01 | 0.7529 | 2.5981 |

Fig. 12 shows the control errors from the reference optimal control with a ±20% model uncertainty.

Table 4 shows that increasing the model uncertainty, i.e., the system matrix $\mathbf{A}(t)$, changes the velocities. However, the final position and velocity errors are all similar to the normal value. Therefore, the present guidance law can overcome the impact of model uncertainty and satisfactorily track the nominal reference trajectory and control. This conclusion can also be obtained from Figs. (10)–(12); with a ±20% model uncertainty in the system matrix $\mathbf{A}(t)$, the trajectory, velocity and control input errors are all similar to the nominal reference values, and they all converge to the nominal reference values.

### 5.3. Effect of the guidance law parameter

In the two previous sections, the effectiveness and robustness of the proposed guidance law were validated using numerical simulations that included initial velocity errors and model uncertainties. The efficiency of the guidance law is also important in the real implementation of transfer missions. Although the generating function method for solving the receding horizon control problem can efficiently solve the equivalent form of the Riccati differential equation and does not require the online direct integration of the original Riccati differential equation, the computational efficiency also needs to be validated. To compare the ability of the real-time implementation of the receding horizon control method, a Riccati transformation-based backward sweep method (Bryson and Ho, 1975; Ohtsuka and Fujii, 1997) is used to solve the same problem. The method used is to solve the Riccati differential equation at every time step.

The parameters in the numerical simulations are chosen as follows. The flight time is 120 days, and the initial velocity errors are all 10 m/s. The results obtained from the generating function method and the backward sweep method with different values of the receding horizon control parameter $T$ are given in Table 5. Table 5 also shows the

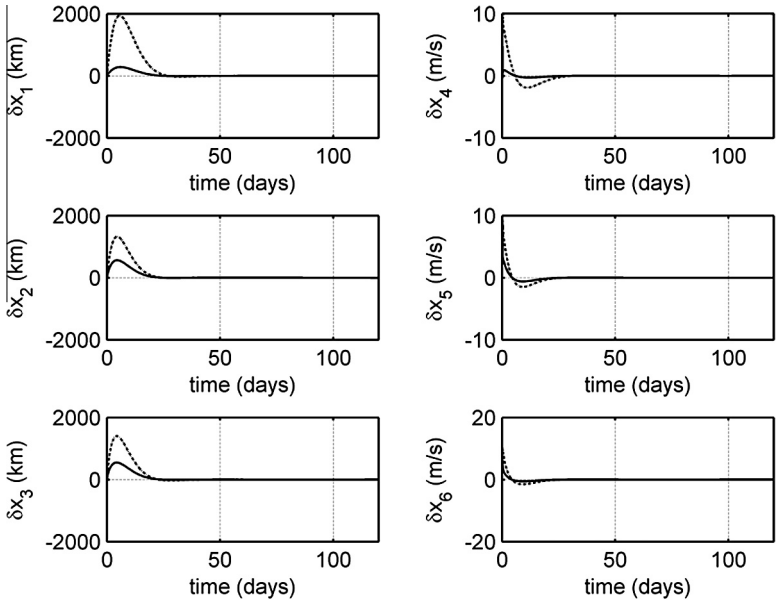


Fig. 13. Errors from the optimal reference trajectory for the GF (solid line) and BS (dashed line) methods.

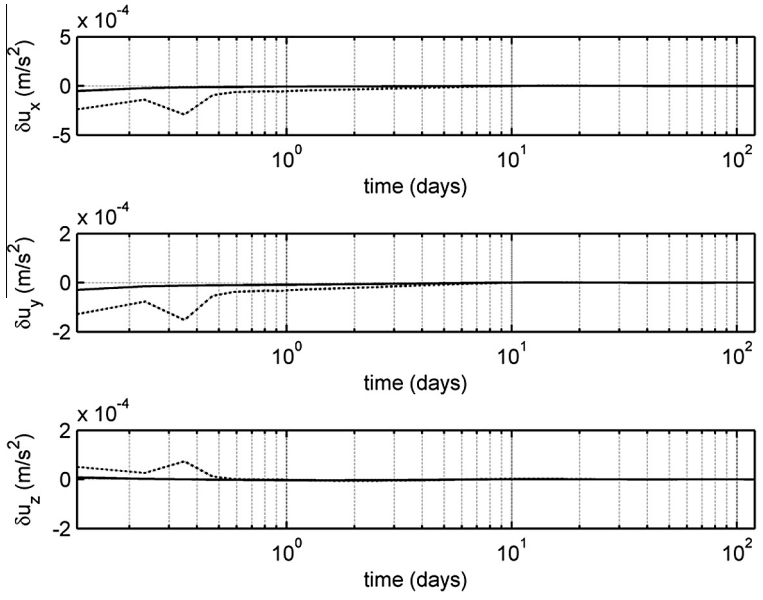


Fig. 14. Errors from the optimal reference control for the GF (solid line) and BS (dashed line) methods.

total CPU time consumption $T_{\text{cpu}}$, the velocity change $\Delta V$ and the final position (velocity) errors $\Delta e_p$ ($\Delta e_v$). "GF" and "BS" are abbreviations for "Generating Function" and "Backward Sweep", respectively. Many conclusions can be obtained from Table 5. First, the CPU times for the GF method remain nearly constant with increases of $T$. However, the CPU times for the BS method increase significantly with increasing values of $T$. The computational efficiency of the GF method is at least one order of magnitude better than the BS method for the same value of $T$. Secondly, the velocity change of the GF method decreased at first and then increased with increases of $T$. The velocity change of the BS method has no obvious statistical characteristics and has many local minima. In general, the GF method gives smaller fuel expenditures than the BS method for the same value of $T$ (except for the first line). The GF and BS methods give final position (velocity) errors $\Delta e_p$ ($\Delta e_v$) with precisions of the same order of magnitude. However, the precision of the GF method becomes better than the BS method at larger values of $T$.

Figs. 13 and 14 show the errors from the reference trajectory and control for $T = 10$ for the GF and BS methods, respectively. The solid lines denote the results from the GF method, and the dashed lines denote the results from the BS method. The errors from the optimal reference trajectory and control for the GF method and the BS method

converge quickly. However, the GF method has smaller deviations than the BS method in the convergence process, especially for the position errors. Finally, the maximum value of control input for the GF method is smaller than that in the BS method.

## 6. Conclusions

This study examines the problem of transferring a spacecraft with low thrust from a near-Earth orbit to a halo orbit around the libration point $L_2$ in the Sun–Earth system. A guidance law based on the receding horizon control method is proposed to study the guidance problem using the nonlinear bicircular four-body model. Using the launch velocity errors and the uncertainties of the nonlinear model, the guidance law is implemented to compensate for deviations from the optimal reference trajectory. The effect of the initial injection condition and the guidance law parameters are studied in detail using numerical simulations. The results of the numerical simulations demonstrate the capabilities of the proposed guidance law. The generating function method for solving the receding horizon control problem has an advantage over the backward sweep method, which is based on the online integration of the Riccati differential equation. The generating function method results in a one order of magnitude improvement in computational efficiency over the backward sweep method.

## Acknowledgments

The authors are grateful to the financial supports of the National Science Foundation of China (11102031, 11272076, 11072044).

## References

Arrieta-Camacho, J.J., Biegler, L.T. Real time optimal guidance of low-thrust spacecraft: an application of nonlinear model predictive control. Ann. NY. Acad. Sci. 1065, 174–188, 2005.

Assadian, N., Pourtakdoust, S.H. Multiobjective genetic optimization of Earth–Moon trajectories in the restricted four-body problem. Adv. Space Res. 45 (3), 398–409, 2010.

Breakwell, J.V., Kamel, A.A., Ratner, M.J. Station-keeping for a translunar communication station. Celest. Mech. Dyn. Astron. 10, 357–373, 1974.

Bryson Jr, A.E., Ho, Y.C. Applied Optimal Control: Optimization, Estimation and Control. Taylor and Francis, 1975.

Betts, J.T. Survey of numerical methods for trajectory optimization. J. Guid. Control Dyn. 21 (2), 193–207, 1998.

Biegler, L.T. Nonlinear programming: concepts, algorithms, and applications to chemical processes. SIAM Society for Industrial and Applied Mathematics, Philadelphia, 2010.

Conley, C.C. Low energy transit orbits in the restricted three body problem. SIAM J. Appl. Math. 16, 732–746, 1968.

Cabette, R.E.S., Prado, A.F.B.A. Transfer orbits to/from the Lagrangian points in the restricted four body problem. Acta Astronaut. 63 (11–12), 1221–1232, 2008.

Conway, B.A. A survey of methods available for the numerical optimization of continuous dynamic systems. J. Optimiz. Theory Appl., http://dx.doi.org/10.1007/s10957-011-9918-z, 2011.

Circi, C. Properties of transit trajectory in the restricted three and four-body problem. Adv. Space Res. 49 (10), 1506–1519, 2012.

Davison, E.J., Maki, M.C. The numerical solution of the matrix Ricatti differential equation. IEEE Trans. Autom. Control 18 (1), 71–73, 1973.

Dellnitz, M., Ober-Blöbaum, S., Post, M., et al. A multi-objective approach to the design of low thrust space trajectories using optimal control. Celest. Mech. Dyn. Astron. 105 (1–3), 33–59, 2009.

Farquhar, R.W. The control and use of libration-point satellites, NASA. TR. R-346, 1970a.

Farquhar, R.W. The utilization of halo orbits in advanced lunar operations, Goddard Space Flight Center, X-551-70-449, 1970b.

Farquhar, R.W., Muhonen, D.P., Newman, C.R., et al. Trajectories and orbital maneuvers for the first libration-point satellite. J. Guid. Control Dyn. 3 (6), 549–554, 1980.

Farquhar, R.W., Dunham, D.W., Guo, Y., et al. Utilization of libration points for human exploration in the Sun–Earth–Moon system and beyond. Acta Astronaut. 55 (3–9), 687–700, 2004.

Gómez, G., Lo, M.W., Masdemont, J.J. Libration Point Orbits and Applications, World Scientific Publishing, 2003.

Gómez, G., Marcote, M., Masdemont, J.J. Trajectory correction manoeuvres in the transfer to libration point orbits. Acta Astronaut. 56 (7), 652–669, 2005.

Howell, K.C., Pernicka, H.J. Stationkeeping method for libration point trajectories. J. Guid. Control Dyn. 16 (1), 151–159, 1993.

Hiday-Johnston, L.A., Howell, K.C. Transfers between libration-point orbits in the elliptic restricted problem. Celest. Mech. Dyn. Astron. 58, 317–337, 1994.

Hull, D.G. Conversion of optimal control problems into parameter optimization problems. J. Guid. Control Dyn. 20 (1), 57–60, 1997.

Howell, K.C., Barden, B., Lo, M. Application of dynamical systems theory to trajectory design for a libration point mission. J. Astronaut. Sci. 45 (2), 161–178, 1997.

Hairer, E., Lubich, C., Wanner, G. Geometric Numerical Integration: Structure-Preserving Algorithm for Ordinary Differential Equations. Springer, New York, 2006.

Kwon, W.H., Pearson, A.E. A modified quadratic cost problem and feedback stabilization of a linear system. IEEE Trans. Autom. Control 22 (5), 838–842, 1977.

Kechichian, J.A. Computational aspects of transfer trajectories to halo orbits. J. Guid. Control Dyn. 24 (4), 796–804, 2001.

Kulkarni, J.E., Campbell, M.E., Dullerud, G.E. Stabilization of spacecraft flight in halo orbits: an H$\infty$ approach. IEEE Trans. Control Syst. Technol. 14 (3), 572–578, 2006.

Lu, P. Regulation about time-varying trajectories: precision entry guidance illustrated. J. Guid. Control Dyn. 22 (6), 784–790, 1999.

Lu, P. Closed-form control laws for linear time-varying systems. IEEE Trans. Autom. Control 45 (3), 537–542, 2000.

Li, M.T., Zheng, J.H. Impulsive lunar halo transfers using the stable manifolds and lunar flybys. Acta Astronaut. 66 (9–10), 1481–1492, 2010.

Mingotti, G., Topputo, F., Bernelli-Zazzera, F. Combined optimal low-thrust and stable-manifold trajectories to the Earth-Moon halo orbits, in: New Trends in Astrodynamics and Applications III, AIP Conference Proceedings, vol. 886, 100-112, 2007.

Mingotti, G., Topputo, F., Bernelli-Zazzera, F. Efficient invariant-manifold, low-thrust planar trajectories to the Moon. Commun. Nonlinear Sci. 17 (2), 817–831, 2012.

Ohtsuka, T., Fujii, H.A. Real-time optimization algorithm for nonlinear receding-horizon control. Automatica 33 (6), 1147–1154, 1997.

Ozimek, M.T., Howell, K.C. Low-thrust transfers in the Earth–Moon system, including applications to libration point orbits. J. Guid. Control Dyn. 33 (2), 533–549, 2010.

Park, C., Guibout, V., Scheeres, D.J. Solving optimal continuous thrust rendezvous problems with generating functions. J. Guid. Control Dyn. 29, 321–331, 2006.

Peng, H.J., Gao, Q., Wu, Z.G., et al. Symplectic adaptive algorithm for solving nonlinear two-point boundary value problems in astrodynamics. Celest. Mech. Dyn. Astron. 110 (4), 319–342, 2011.

Richardson, D.L. Analytic construction of periodic orbits about the collinear points. Celest. Mech. Dyn. Astron. 22 (3), 241–253, 1980.

Rausch, R.R. Earth to halo orbit transfer trajectories, M.S. Thesis, School of Aeronautics and Astronautics, Purdue University, West Lafayette, Indiana, 2005.

Ross, I.M. Space trajectory optimization and L1-optimal control problems. In: Gurfil, P. (Ed.), Modern Astrodynamics. Elsevier, St.Louis, MO, pp. 155–188 (Chapter 6), 2006.

Romagnoli, D., Circi, C. Lissajous trajectories for lunar global positioning and communication systems. Celest. Mech. Dyn. Astron. 107 (4), 409–425, 2010.

Schaub, H., Junkins, J.L. Analytical Mechanics of Aerospace Systems, AIAA Education Series, 2002.

Serban, R., Koon, W.S., Lo, M.W., et al. Halo orbit mission correction maneuvers using optimal control. Automatica 38 (4), 571–583, 2002.

Salmani, M., Büskens, C. Real-time control of optimal low-thrust transfer to the Sun–Earth L1 halo orbit in the bicircular four-body problem. Acta Astronaut. 69 (9–10), 882–891, 2011.

Tantardini, M., Fantino, E., Ren, Y., et al. Spacecraft trajectories to the L3 point of the Sun–Earth three-body problem. Celest. Mech. Dyn. Astron. 108 (3), 215–232, 2010.

Tian, B., Zong, Q. Optimal guidance for reentry vehicles based on indirect Legendre pseudospectral method. Acta Astronaut. 68 (7–8), 1176-1134, 2011.

Wang, S.K., Lo, M.W., Marsden, J.E. et al., Dynamical Systems, the Three-Body Problem and Space Mission Design, Springer, 2007.

Wu, Z.G., Zhong, W.X. A structure-preserving algorithm for the minimum H$\infty$ norm computation of finite-time state feedback control problem. Int. J. Control 82 (4), 773–781, 2009.

Wu, Z.G., Mesbahi, M. Symplectic transformation based analytical and numerical methods for linear quadratic control with hard terminal constraints. SIAM J. Control Optim. 50 (2), 652–671, 2012.

Xu, M., Xu, S.J. Trajectory and correction maneuver during the transfer from Earth to halo orbit. Chin. J. Aeronaut. 21 (3), 200–206, 2008.

Zanzottera, A., Mingotti, G., Castelli, R., et al. Intersecting invariant manifolds in spatial restricted three-body problems: design and optimization of Earth-to- halo transfers in the Sun–Earth–Moon scenario. Commun. Nonlinear Sci. 17 (2), 832–843, 2012.